

REVIEW ARTICLE

# Two-dimensional MXenes: New frontier of wearable and flexible electronics

Abbas Ahmed<sup>1</sup> | Sudeep Sharma<sup>2</sup> | Bapan Adak<sup>3</sup>  | Md Milon Hossain<sup>4,5</sup> | Anna Marie LaChance<sup>1,6</sup> | Samrat Mukhopadhyay<sup>3</sup> | Luyi Sun<sup>1,6</sup> 

<sup>1</sup>Polymer Program, Institute of Materials Science, University of Connecticut, Storrs, Connecticut, USA

<sup>2</sup>Advanced Sensor and Energy Research (ASER) Lab, Department of Electronic Engineering, Kwangwoon University, Seoul, South Korea

<sup>3</sup>Department of Textile and Fiber Engineering, Indian Institute of Technology, New Delhi, India

<sup>4</sup>Department of Textile Engineering, Chemistry and Science, North Carolina State University, Raleigh, North Carolina, USA

<sup>5</sup>Department of Textile Engineering, Khulna University of Engineering & Technology, Khulna, Bangladesh

<sup>6</sup>Department of Chemical and Biomolecular Engineering, University of Connecticut, Storrs, Connecticut, USA

## Correspondence

Bapan Adak, Department of Textile and Fiber Engineering, Indian Institute of Technology, New Delhi 110016, India.  
Email: bapan.iitd15@gmail.com

Md Milon Hossain, Department of Textile Engineering, Chemistry and Science, North Carolina State University, Raleigh, NC 27606, USA.  
Email: mhossai5@ncsu.edu

Samrat Mukhopadhyay, Department of Textile and Fiber Engineering, Indian Institute of Technology, New Delhi 1100616, India.  
Email: samrat.mukhopadhyay@textile.iitd.ac.in

Luyi Sun, Polymer Program, Institute of Materials Science, University of Connecticut, Storrs, CT 06269, USA.  
Email: luyi.sun@uconn.edu

## Abstract

Wearable electronics offer incredible benefits in mobile healthcare monitoring, sensing, portable energy harvesting and storage, human-machine interactions, etc., due to the evolution of rigid electronics structure to flexible and stretchable devices. Lately, transition metal carbides and nitrides (MXenes) are highly regarded as a group of thriving two-dimensional nanomaterials and extraordinary building blocks for emerging flexible electronics platforms because of their excellent electrical conductivity, enriched surface functionalities, and large surface area. This article reviews the most recent developments in MXene-enabled flexible electronics for wearable electronics. Several MXene-enabled electronic devices designed on a nanometric scale are highlighted by drawing attention to widely developed nonstructural attributes, including 3D configured devices, textile and planer substrates, bioinspired structures, and printed materials. Furthermore, the unique progress of these nanodevices is highlighted by representative applications in healthcare, energy, electromagnetic interference (EMI) shielding, and humanoid control of machines. The emerging prospects of MXene nanomaterials as a key frontier in next-generation wearable electronics are envisioned and the design challenges of these electronic systems are also discussed, followed by proposed solutions.

## KEYWORDS

flexible electronics, MXene, nanostructures, wearable electronics

## 1 | INTRODUCTION

Due to recent advances in wearable technologies and smart electronics, flexible and miniaturized devices have attracted exponential attention by bringing a new product paradigm into consumer electronics. These advances in wearable technologies have provided enormous access to flexible electronics for applications in intelligent health and home appliances, self-powered devices, smart displays and sensors, soft-robotics, human-machine interactions, etc.<sup>1–9</sup> Impressively, the current development of flexible electronic devices can be realized from their intrinsic characteristics, such as being lightweight, cost-effective, and easy to mount on skin.

In healthcare, the natural interactions between electronics and the human body to measure and collect data from the human body will one day make wearable electronics ubiquitous in the industry. Therefore, the materials should be durable, conformable to human skin, and sustainable for noninvasive monitoring<sup>10–12</sup> which is highly desirable in electronic sensing platforms where the presence of a human body is expected. In recent years, great strides have been made in wearable electronics incorporating various organic and inorganic nanomaterials for functional applications.<sup>13,14</sup> Although significant progress has been made in nanomaterial electronics to operate reliably and smoothly over a human body, concerns about biocompatibility and device efficiency are constantly under consideration. Interestingly, more advanced devices extensively explore the use of different nanomaterials.

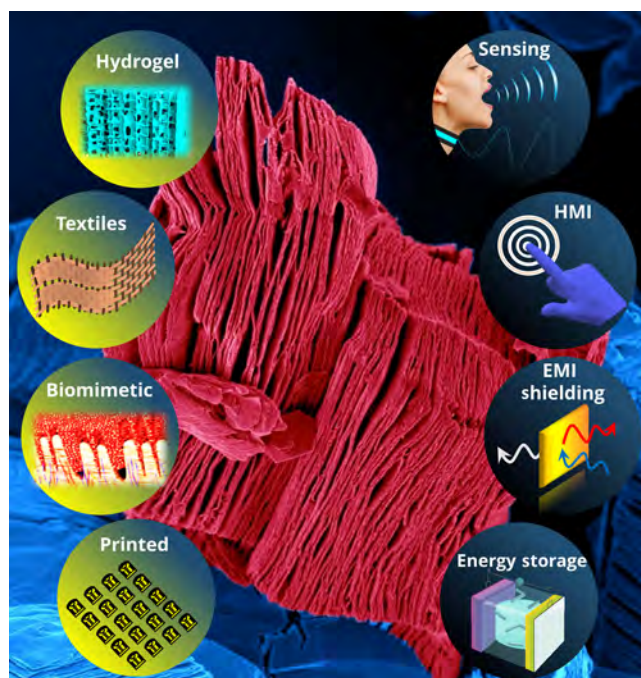
Two-dimensional (2D) nanomaterials have been widely adopted for the development of flexible electronics for widespread applications. Among other 2D materials, the newly emerged MXenes have attracted considerable attention in the design and development of flexible electronics. 2D MXenes are the layered transition metal carbides or nitrides and synthesized from  $M_{n+1}AX_n$  (MAX) phase precursors, where M is an early metal, A is an element from group IIIA or IVA in the periodic table, X is carbon/nitrogen and the value of  $n$  is 1–3.<sup>15–17</sup> Naguib et al.<sup>18</sup> first synthesized  $Ti_3C_2T_x$  by hydrofluoric acid (HF)-assisted selective etching of the Al layer from the  $Ti_3AlC_2$  MAX phase precursor. The  $T_x$  in the MXene formula refers to various surface terminal functional groups (such as  $-O$ ,  $-OH$ ,  $-F$ ,  $-Cl$ ), obtained through different synthesis processes. The properties of MXenes can be tailored by modifying M or X elements and the surface functionalities.<sup>19–23</sup> MXenes have high electrical conductivity, excellent electrochemical and optoelectronic properties, and tunable surface functionality. Specifically, higher electrical conductivity and tunable surface functional groups have enabled MXenes to be used in several

electronic systems, for instance, in advanced healthcare systems,<sup>2,24</sup> flexible electronics,<sup>25–27</sup> and wearable energy-related fields.<sup>28–34</sup> The enriched structural features of MXene enable the fabrication of devices from bioinspired sources<sup>35,36</sup> and their integration into textile or planar substrates for wearable electronics,<sup>15,37,38</sup> realizing various geometries such as smart textile-based devices, printed electronic devices, and 3D-configured devices (e.g., aerogels and hydrogels) for functional applications.<sup>24,39–42</sup> Moreover, the improved coupling and hybridization of MXene with other materials at the nanoscale makes it one of the most intriguing materials for wearable applications.<sup>43</sup> The next few years are expected to witness tremendous progress in efficiently producing and handling MXene-based nanoelectronic materials. However, issues with scalable synthesis, oxidation, aggregation in specific solvent systems, and poor mechanical properties should be addressed for the design of MXene-based functional electronic devices.

This progress report summarizes the latest advancements in nanoengineered MXene-based flexible electronics for wearable applications. First, the advances in functional nanostructures derived from MXene are discussed, providing insights into their various preparation strategies. In addition, several critical morphological features of such nanostructures are also elucidated. In the next section, various system-level applications, for example, energy storage and harvesting, electromagnetic interference (EMI) shielding, healthcare, and human-machine interfacing (HMI) based on MXene nanodevices are exemplified. Figure 1 illustrates the significant applications of MXene-based wearable flexible devices. The review concludes by highlighting several challenges and envisioning new opportunities for MXene-based wearable and flexible electronics.

## 2 | MECHANICAL AND ELECTRICAL CHARACTERISTICS OF MXENE

Experimental results revealed that the Young's modulus of individual single-layer  $Ti_3C_2T_x$  was  $330 \pm 30$  GPa, much higher than that of 2D graphene oxide (GO) and graphene oxide (rGO).<sup>46</sup> Meanwhile, the tensile strength at break of a single-layer of  $Ti_3C_2T_x$  was  $17.3 \pm 1.6$  GPa. These results are in agreement with the theoretical predictions by the density functional theory (DFT).<sup>47</sup> Moreover, the transition elements present in the MXene structure largely influence the mechanical properties, and the intrinsic tensile behavior can be further modified by tailoring the surface of MXene. For example, Nb-based single-layer  $Nb_4C_3T$  MXene exhibited a Young's modulus



**FIGURE 1** Schematic representing the excellent and emerging avenues of MXene electronics for wearable energy storage, EMI shielding, flexible sensing, and HMI. MXene SEM image credit: Prof. Babak Anasori (IUPUI) and Prof. Yury Gogotsi, Drexel University, USA. MXene hydrogel. Reproduced with permission.<sup>44</sup> Copyright 2018, the American Chemical Society. MXene biomimetic structure. Reproduced with permission.<sup>45</sup> Copyright 2020, the American Chemical Society. EMI, electromagnetic interference; HMI, human-machine interfacing

of  $386 \pm 14$  GPa, which is higher than Ti-based single-layer  $\text{Ti}_3\text{C}_2\text{T}_x$  MXene.<sup>48</sup>

The effect of layer thickness on the mechanical properties of 2D  $\text{Ti}_{n+1}\text{C}_n$  was evaluated by molecular dynamics (MD) calculations, where decreasing the layer thickness resulted in an increase in Young's modulus of MXenes. The Young's moduli of  $\text{Ti}_2\text{C}$ ,  $\text{Ti}_3\text{C}_2$ , and  $\text{Ti}_4\text{C}_3$  were found to be 597, 502, and 534 GPa, respectively, which demonstrated that the thinnest  $\text{Ti}_2\text{C}$  carbide composed of three atomic layers had the highest Young's modulus.<sup>49</sup> Similar results by another group also showed that increasing the single-layer thickness of MXene led to a decrease in Young's modulus.<sup>50</sup>

MXene offers excellent electrical conductivities that are the highest among other solution-processed 2D materials.<sup>51,52</sup> Surprisingly, with the addition of various M and X elementals and a controlled synthesis process, MXene may possess electrical conductivities as high as  $20\,000\text{ S cm}^{-1}$ .<sup>51</sup> Individual single-layer  $\text{Ti}_3\text{C}_2\text{T}_x$  nanosheets demonstrate a high electrical conductivity of ca.  $4600\text{ S cm}^{-1}$ .<sup>53</sup> One of the key factors that affect the electrical properties of MXene is

the M-layer. Thus, by maintaining a delicate balance between temperature and the activity of etchants, the electrical properties from metallic to semiconductor can be modulated by changing the outer transition layer of 2D carbide. In addition, the presence of various etchants, defects, and surface termination groups during MXene synthesis can also play a crucial role in its electrical conductivity. For example, experiments have showed that the conductivity of HF-etched  $\text{Ti}_3\text{C}_2\text{T}_x$  powder is almost  $1000\text{ S cm}^{-1}$ , which is about five times lower than that of  $\text{Ti}_3\text{C}_2$  nanosheets with few defects ( $6500\text{ S cm}^{-1}$ ).<sup>43,54</sup>

### 3 | MXENE-ENABLED DEVICE ARCHITECTURES

#### 3.1 | Textile and planar structures

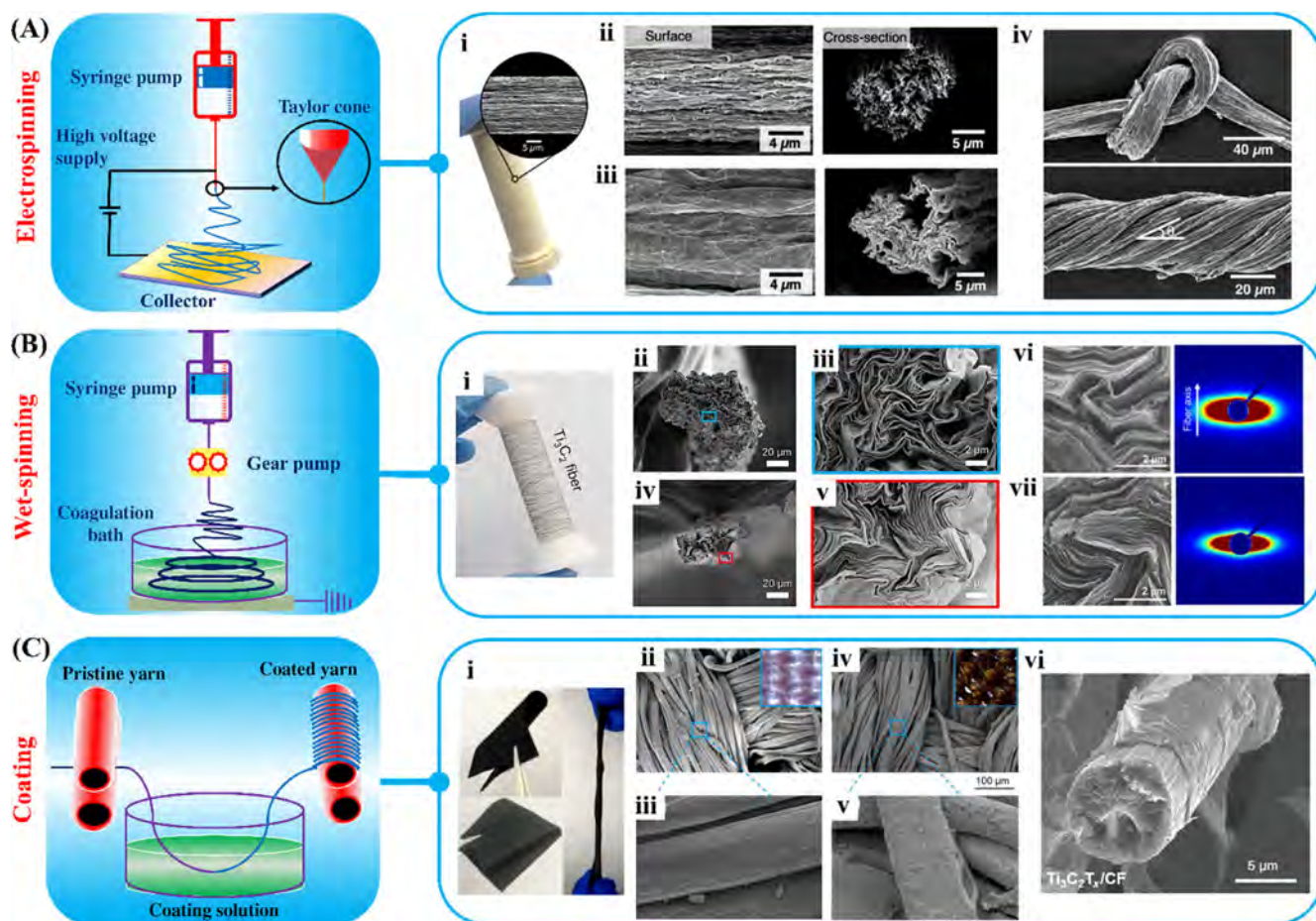
With their outstanding flexibility for skin-mountable and wearable electronics, smart-textiles have seen an exponential increase in the diversity of their applications. Textiles started out as esthetic, everyday consumables, but have become advanced, demanding constructs for modern wearable technologies. These revolutionary advances and modifications in textiles have been made possible with the emergence of nanomaterials including graphene,<sup>11,55,56</sup> MXene,<sup>15,57,58</sup> carbon nanotubes (CNTs),<sup>59</sup> conducting polymers,<sup>60</sup> metallic nanoparticles/nanowires,<sup>61,62</sup> and so on. Textile-based electronic devices have been widely used in flexible, portable energy storage and conversion systems,<sup>63,64</sup> real-time healthcare monitoring,<sup>65–68</sup> flexible sensing,<sup>69–73</sup> flexible displays,<sup>4</sup> thermal management,<sup>74–77</sup> biomedical therapy,<sup>78</sup> soft-robotics,<sup>79,80</sup> and so on. Although several nanomaterials have enabled smart textiles for wearable electronics, novel 2D MXene has recently received more attention. The surface functional groups of MXene can directly bond with the fiber and impart functionality to the insulating textiles. Furthermore, the ease of solution processing and mechanical flexibility have made MXene an ideal candidate for smart textile manufacturing,<sup>15</sup> offering multifaceted material morphologies and structures for wearable applications.

MXene has versatile processability, for example, it can be mixed into different spinning dopes to produce purely electro-spun or wet-spun MXene fibers, or can be coupled as a secondary dopant in spinning dope to produce smart composite fibers.<sup>15</sup> These excellent potentials for MXene treatment are attributed to its ability to disperse in a variety of solvents, including water, dimethyl sulfoxide (DMSO), dimethylformamide (DMF), *N*-methyl-2-pyrrolidone (NMP). Notably, among other MXene smart textile processing techniques, several coating techniques (spray-coating, dip-coating, etc.) have



been widely explored because of their ease of processing and scalability.<sup>52</sup> In addition, the many surface functional groups on MXene and the tunable rheological properties of MXene suspensions facilitate its processing in various printing techniques (mostly in screen-printing, inkjet printing, and 3D printing). A detailed discussion of different MXene-enabled printing processes can be found in Section 3.4. Maintaining suitable MXene flake size is an extremely crucial factor as improper flake size may compromise smart-textile production and lead to deterioration in material performance.<sup>15</sup> For instance, small flakes

of MXene nanosheets conformally coat the core and inter-stitches of fibers and yarns, but compromises electrical conductivity, which is key to many electronic applications. On the other hand, coating of fibers with large MXene flakes induces higher electrical conductivity but offers poor adherence to fiber surfaces and deteriorates mechanical flexibility.<sup>81</sup> Therefore, the size of the MXene flakes should be optimized according to the desired applications, especially for textile-based supercapacitor electrodes (SCs). Overall, to develop an efficient MXene-mediated textile interface, functionalization of textile



**FIGURE 2** (A) Schematic of the electrospinning process. (i) Photograph showing MXene/nylon nano yarns. The inset exhibits a SEM image of MXene/nylon nano yarns. Surface and cross-sectional SEM images of MXene nano yarns prepared using MXene flake size and concentration (ii)  $\sim 220$  nm at  $10 \text{ mg mL}^{-1}$  and (iii)  $\sim 850$  nm at  $10 \text{ mg mL}^{-1}$ . (iv) SEM image of a knotted and twisted MXene/nylon nano yarn produced from  $10 \text{ mg mL}^{-1}$ ,  $220$  nm flakes. Reproduced with permission.<sup>82</sup> Copyright 2020, WILEY-VCH Verlag. (B) Illustration of wet-spinning process. (i) Photograph of a 5-m long  $\text{Ti}_3\text{C}_2$  fiber wound on a spool. (ii, iii) Cross-sectional SEM images of LC MXene fibers prepared from an acetic acid bath solution using S- $\text{Ti}_3\text{C}_2$  flakes. (iv, v) SEM images showing a cross-section of fibers prepared from a chitosan bath solution using S- $\text{Ti}_3\text{C}_2$  flakes. Reproduced with permission.<sup>83</sup> Copyright 2021, the American Chemical Society. (vi, vii) SEM image and SAXS patterns of MXene fibers. Reproduced with permission.<sup>84</sup> Copyright 2021, the American Chemical Society. (C) Schematic of the coating process. (i) Folding and bending properties of MXene impregnated cotton fabrics. (ii, iii) SEM images of pristine cotton fabrics, (iv, v) 6 wt% MXene impregnated cotton fabrics. Reproduced with permission.<sup>85</sup> Copyright 2020, the American Chemical Society. (vi) SEM image of  $\text{Ti}_3\text{C}_2\text{T}_x$  flakes coated on a carbon fabrics fiber. Reproduced with permission.<sup>86</sup> Copyright 2018, WILEY-VCH Verlag. LC, liquid crystalline; SAXS, small-angle X-ray scattering; SEM, scanning electron microscopy

surfaces is critical and MXene should be synthesized, modified, and optimized according to applications.

Currently, three widely-explored textile processing techniques have been investigated to produce MXene mediated fibers/yarns and fabrics: (i) electrospinning, (ii) wet-spinning, and (iii) coating. A schematic demonstration of each process is depicted in Figure 2A–C. As an effective nanofiller, MXene has been incorporated into several polymer-based spinning solutions to function as a co-dopant, resulting in nanofibers with multifunctionalities in contrast to the pristine polymer-based spun fibers. For example, a unique combination of both electrospinning and wet-spinning has been established by Levitt and co-workers<sup>82</sup> to produce MXene-infiltrated nylon nano yarns. This combined spinning process enabled the dispersion of MXene nanoflakes throughout the entire cross-sections of nano yarns, and achieved an all-time highest MXene loading (90%) in terms of spinning processing. MXene flake size affect the fiber spinning process and displays significant morphological changes in microstructure. The nano yarns spun with a small flake size (220 nm) revealed a circular microstructure, but larger MXene flakes (850 nm) demonstrated randomly-oriented fibers with intertwined MXene flakes at a relatively low MXene concentration (10 mg mL<sup>-1</sup>; Figure 2A(i–iii)). Furthermore, the electrospun nano yarns produced from small flakes (220 nm at 10 mg mL<sup>-1</sup>) exhibited mechanical integrity and no obvious morphological changes were observed after knotting the yarn (Figure 2A(iv)). Finally, the nano yarns showed promise to be used as a SC. In another study, Levitt et al.<sup>87</sup> embedded delaminated MXene flakes into a polyacrylonitrile (PAN) electrospinning dope, whose spun fibers were carbonized in an argon atmosphere at different temperatures. Incorporating carbon in nanofiber materials with their efficient ion diffusion paths significantly improved the electrochemical performance due to small fiber diameter and electrical conductivity. Several MXene-reinforced electrospun nanofibers have been produced for SCs, showing excellent avenues in the fiber-based energy-storage platform.

The excellent dispersibility in different polar solvents, liquid crystalline (LC) behavior, pseudoelasticity, and the tunable rheological properties of MXene facilitates wet spinning to produce neat MXene fibers or MXene-based composite fibers. For example, by imparting LC behavior in Ti<sub>3</sub>C<sub>2</sub> MXene, a pure wet spun MXene fiber was developed by Zhang et al.<sup>83</sup> for fiber-shaped SC and flexible heating elements for thermal devices (Figure 2B(i)). The fiber formation process studied multiple parameters, including MXene flake size, concentration, types of coagulation bath, and needle gauge, etc. For instance, fibers produced from an acetic acid bath containing small Ti<sub>3</sub>C<sub>2</sub>

flakes showed an open microstructural morphology, whereas a densely packed microstructure was observed from chitosan coagulant solution containing large Ti<sub>3</sub>C<sub>2</sub> flakes (Figure 2B(ii–v)).

Interestingly, apart from Ti<sub>3</sub>C<sub>2</sub> MXene, other types of MXene, such as Mo<sub>2</sub>Ti<sub>2</sub>C<sub>3</sub> showed similar microstructural morphology when wet spun with smaller flake size in a chitosan bath. This ease of control in the microstructural assembly of pure MXene fibers allows one to tailor the property of fibers. Collectively, the LC MXene fiber prepared in chitosan bath showed an excellent electrical conductivity (>7748 S cm<sup>-1</sup>), close to free-standing MXene film (ca. 9500 S cm<sup>-1</sup>), resulting in high-throughput electrochemical performance.

Shin et al.<sup>84</sup> designed an effective two-way strategy to develop a mechanically strong Ti<sub>3</sub>C<sub>2</sub>T<sub>x</sub> MXene fiber employing a deformable MXene gel. First, a highly-reinforced MXene gel was prepared from a MXene dispersion wherein the gel network was strengthened by electrostatic interactions between MXene sheets in a basic solution. Then, the MXene dispersion was wet-spun in a coagulation bath to produce gel fibers, making highly-oriented fibers ascribed from the strong gel network. Moreover, during the mechanical drawing, the gel-spun fibers exhibited a capability to withstand high shear stress. With the increase in fiber draw ratios from 1 to 3, a highly-packed lamellar structure and anisotropic streak pattern was observed from the morphological and small-angle X-ray scattering (SAXS) analyses. These results revealed needle-sized microvoids inside the MXene fibers (Figure 2B(vi,vii)). Further analysis on density and porosity demonstrated MXene fiber formation with a denser structure, and the obtained highly-aligned fibers showed extremely enhanced properties, that is, tensile strength (344 MPa), Young's modulus (122 GPa), and electrical conductivity (12 504 S cm<sup>-1</sup>).

In contrast to other MXene textile fiber/yarn and fabric processing techniques, coating is extensively studied owing to facile fabrication strategies and bulk-scale production opportunities. MXene depicts excellent conformal coating of various textile materials such as fibers, yarns, and fabrics, because of its ease in solution processing.<sup>15</sup> Apart from widely performed dip-coating techniques, drop-casting<sup>85</sup> or spray-coating<sup>88</sup> was used for coating MXene on textiles. These processes facilitate a high degree of MXene loading and impart new functional properties. A range of natural and synthetic textiles have been coated with MXene.<sup>85,89,90</sup> For instance, an interwoven natural cotton textile was spray-coated by MXene for multifunctional wearable electronic applications such as Joule heating, EMI shielding, and strain sensing (Figure 2C(i)).<sup>85</sup> The morphological investigation of composite textiles revealed a relatively rough cotton surface with an

increase in MXene content compared to the pristine cotton fabrics (Figure 2C(ii–v)). This enabled an interconnected conductive network within the textile fabrics, which is essential to several electronic applications. During drop-casting, carbon fabrics were wrapped with a  $\text{Ti}_3\text{C}_2\text{T}_x$  dispersion which was used in SC.<sup>86</sup> The coated carbon fiber exhibited a uniform wrapping of  $\text{Ti}_3\text{C}_2\text{T}_x$  MXene flakes over the individual fiber surface (Figure 2C(vi)). Such uniformity in structural morphology has been shown to have several benefits in terms of electrical conductivity. In addition, in the fiber coating process, no binders or additives were added, which is highly desired in fabricating binder-free SCs.

MXene-derived smart-textile devices achieved a considerable progress in flexible electronics which can be mainly categorized in four fields: (i) flexible sensing (pressure and strain),<sup>38,85,91–97</sup> (ii) wearable energy storage system,<sup>87,98–103</sup> (iii) thermal therapy,<sup>85,90,104–106</sup> and (iv) EMI shielding.<sup>88,107–111</sup> In additionally, given their excellent processability and device performance, textile integration of MXene-derived smart-textiles has huge promise in wearable electronics for many functional applications, which has enthused scientists around the globe.

### 3.2 | MXene hydrogel assembly and derivatives

Hydrogels are generally composed of water (usually more than 90%) and also contain solvated molecules/polymers and inorganic nanoparticles as gelators in the structure. Hydrogels can retain their distinctive physicochemical properties even in liquid water while presenting a solid-like macroscopically rheological behavior. The three-dimensional (3D) characteristics of hydrogels and their derivatives are attributed to a combination of several chemical and physical interactions. These structures can be created by using 2D nanomaterials as gelators in the presence or absence of polymeric networks.<sup>112</sup> Such structures have enhanced the intrinsic mechanical properties of hydrogels and opened up new possibilities for functional applications.<sup>113,114</sup> MXene has attracted great attention for hydrogel structures, mainly because of their versatile and tunable surface chemistry and exceptional mechanical and hydrophilic characteristics.<sup>115</sup> The remarkable synergies between MXenes and hydrogels are responsible for the enhanced functionalities of MXene-based hydrogels.<sup>112</sup> In addition, functional derivatives of MXene-based hydrogels such as aerogels,<sup>116–119</sup> xerogels,<sup>120</sup> and organohydrogels<sup>121</sup> have been developed, expanding into versatile applications.

MXene hydrogels have found exceptional possibilities in several platforms such as soft and flexible electronics,<sup>116,117</sup> electronic skins,<sup>122</sup> sensors and

actuators,<sup>118,123–126</sup> flexible energy storage,<sup>119,127,128</sup> and biomedicine.<sup>129,130</sup> Although more than 20 different MXenes have been reported so far,  $\text{Ti}_3\text{C}_2\text{T}_x$  has been studied most extensively for hydrogel formation. However, the role of MXene in hydrogels distinctively varies according to the gel structure and gelation mechanisms, having versatile functions such as a self-gelator, co-gelator, crosslinker, and nanofiller. MXene is sometimes assisted by other gelators, which include GO, rGO, polymers, and inorganic ions.<sup>112</sup>

We summarized the inherent properties of MXene hydrogels in Table 1. Moreover, achieving hydrogel materials concerning application-specific properties is regulated by several factors, including MXene concentration, size, and flake thickness. For instance, it was noticed that hydrogels composed of thinner and larger MXene nanosheets exhibit exceptional electrical conductivity and mechanical stability. Particularly, thinner MXene nanosheet-induced hydrogels demonstrate enhanced electrochemical performance compared to MXene hydrogels fabricated from thicker multistacked nanosheets.<sup>119,131</sup> Furthermore, when small and large MXene nanosheets were gelated together, the obtained all-MXene hydrogels exhibited a higher electrochemical performance compared to the hydrogels prepared from similar nanosized sheets alone.<sup>132</sup> This could be due to the high electroconductivity and ionic conductivity of MXene sheets with large and small sizes, respectively. This also signifies that the performance of MXene hydrogels depends not only on their rheology but their 3D microstructure.

Deng et al.<sup>133</sup> reported an MXene hydrogel wherein the MXene gelation process was mediated by divalent metal ions (Figure 3A). The inclusion of  $\text{Fe}^{2+}$  in MXene solution destroys electrostatic repulsion forces between MXene nanosheets, thus assisting in forming a stable 3D hydrogel network. The as-obtained MXene hydrogel depicts enhanced electrochemical performance, attributed to the efficient prevention of restacking of nanosheets during the metal ion-initiated gelation process. A similar 3D hydrogel was prepared for supercapacitor applications utilizing the excellent cross-linking properties of GO and reduction characteristics of ethylenediamine (EDA) that endow dangling oxygen bonds to be formed by oxygen ring-opening. In another report, an MXene nanocomposite organohydrogel was fabricated for strain-sensing applications.<sup>121</sup> In the hydrogel system, first, a nanocomposite hydrogel was prepared using conductive MXene networks into hydrogel polymer networks (Figure 3B). Then the obtained hydrogel was immersed into ethylene glycol solution for the solvent displacement of some of the water molecules. The prepared hydrogel exhibited superior functionality, serving as an anti-freezing and self-healable strain sensor.



**TABLE 1** Summary of the performance and role of MXenes during hydrogel formation

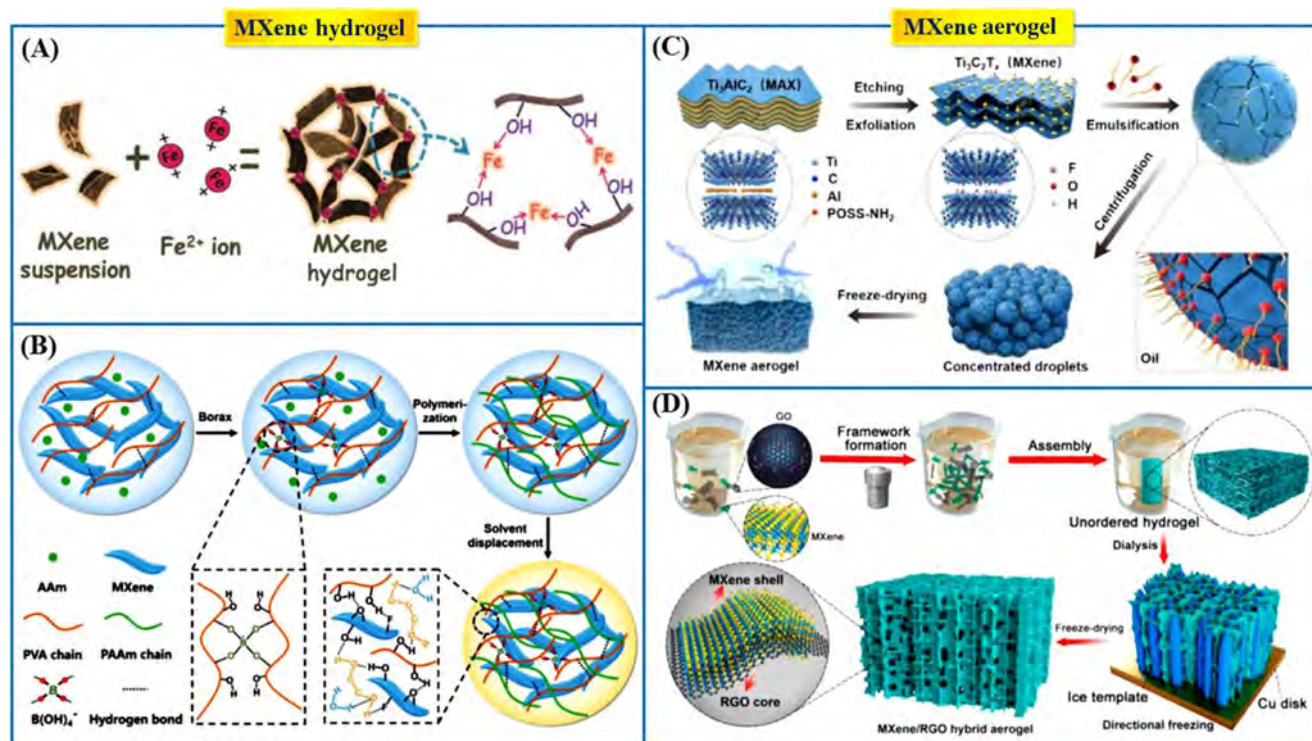
Hydrogel composition	Type and derivative	Synthesis conditions (temperature and time)	Role of MXene	Key features	Application	Ref.
Ti <sub>3</sub> C <sub>2</sub> T <sub>x</sub> /PVA	Hydrogel	20°C, 5 min	Conductive nanofiller, cross-linker	Highly conductive, stretchability (>3400%), moderate stability, GF of 80 under compressive strain	Strain sensing	118
Ti <sub>3</sub> C <sub>2</sub> /GO	Hydrogel	180°C, 6 h	Prevent the restacking of graphene nanosheets	The high specific surface area of 161.1 m <sup>2</sup> g <sup>-1</sup> , energy densities, excellent cycle stability up to 10 000.	Supercapacitor electrode	128
Ti <sub>3</sub> C <sub>2</sub> T <sub>x</sub> /PVA	Hydrogel	90°C, 9.5 h	Conductive nanofiller	Small hysteresis, rapid self-heal ability (~0.15 s), high sensing limit (200%), 5.8% reduction in relative after 10 000 stretch cycles	Strain sensing	122
Ti <sub>3</sub> C <sub>2</sub> /PNIPAM	Hydrogel	10°C, >24 h	Conductive nanofiller, crosslinker	Conductivity 1.092 S m <sup>-1</sup> , good mechanical property: tensile strength 0.4 MPa, 14 times higher stretchability than the original length	Smart compression sensor	125
Ti <sub>3</sub> C <sub>2</sub> T <sub>x</sub>	Ionogel	80°C, 48 h	Self-gelator	Achieved a gravimetric capacitance of 70 F g <sup>-1</sup> at voltage window of 3 V, high power performance.	Supercapacitor electrode	119
Ti <sub>3</sub> C <sub>2</sub> T <sub>x</sub> /GO/EDA	Hydrogel	95°C, >6 h	Co-gelator	Gravimetric capacitance of 370 F g <sup>-1</sup> at 5 A g <sup>-1</sup> and only 2% loss of capacitance after 10 000 cycles	Supercapacitor electrode	127
Ti <sub>3</sub> C <sub>2</sub> T <sub>x</sub> /PAAm/PVA	Organo hydrogel	60°C, >4 h	Cross-linker	Excellent antifreezing at extreme temperature (-40°C), broad strain range (~350%), and GF of 44.85	Strain sensor	121

Abbreviations: EDA, ethylenediamine; GF, gauge factor; GO, graphene oxide; PAAm, polyacrylamide; PNIPAM, poly(*N*-isopropyl acrylamide); PVA, polyvinyl alcohol.

Among other MXene hydrogel derivatives, MXene aerogels are widely explored for various applications, ascribed to their large specific surface area, high porosity, 3D structure, low density, and lightweight properties. Analogous to MXene hydrogels, MXene aerogels simply differ in preparation where sublimation of ice crystals from frozen dispersions or hydrogels are required.<sup>112</sup> So far, several MXene-based aerogel fabrication strategies have been investigated, including freeze-drying of MXene

hydrogels<sup>44</sup> and direct freeze-drying of MXene nanocomposite dispersions.<sup>135,136</sup>

Shi and co-workers<sup>134</sup> prepared an MXene aerogel using a freeze-casting technique through tuning a MXene-surfactant-based Pickering emulsion. At first, a cooperative assembly of Ti<sub>3</sub>C<sub>2</sub>T<sub>x</sub> MXene and oil-soluble amine-functionalized polyhedral oligomeric silsesquioxane (POSS-NH<sub>2</sub>) was formulated in an oil-water system and then jammed of to form an MXene-surfactant. Finally, the



**FIGURE 3** (A) Schematic representation of metal ion-mediated interaction of MXene nanosheets forming MXene aerogel. Reproduced with permission.<sup>133</sup> Copyright 2019, WILEY-VCH Verlag. (B) Schematic illustration of the fabrication process of MXene organohydrogel. Reproduced with permission.<sup>121</sup> Copyright 2019, WILEY-VCH Verlag. (C) Formation of Pickering emulsions and MXene aerogels via MXene surfactants. Reproduced with permission.<sup>134</sup> Copyright 2019, WILEY-VCH Verlag. (D) Schematic showing the construction process of a  $\text{Ti}_3\text{C}_2\text{T}_x$  MXene/rGO hybrid aerogel combining GO-assisted hydrothermal assembly, directional freezing, and freeze-drying. Reproduced with permission.<sup>44</sup> Copyright 2018, the American Chemical Society. GO, graphene oxide; PAAm, polyacrylamide; PVA, polyvinyl alcohol; rGO, reduced graphene oxide

concentrated emulsion was freeze-dried to assemble hydrophobic MXene aerogel (Figure 3C). The produced aerogel offers opportunities for EMI shielding and oil-adsorptions. In another study, Zhao et al.<sup>44</sup> designed a GO-assisted porous 3D MXene aerogel through a combination of hydrothermal assembly, directional freezing, and freeze-drying technique. In this hybrid aerogel, a cellular microstructure was produced where graphene and MXene served as the inner skeleton and shells of the cell wall, respectively (Figure 3D). Benefiting from the excellent gelation capability from GO during the hydrothermal process, enhanced polar interaction occurred between MXene sheets and rGO, which ultimately resulted in a core-shell 3D structure.<sup>44</sup> The core-shell MXene/rGO framework nanocomposite assembled with epoxy had excellent conductivity and EMI shielding performance. Importantly, like MXene hydrogel, the performance of MXene aerogel is largely dependent on MXene concentration, processing method, polymeric molecular weight, etc. A higher MXene concentration promotes disruptive interaction leading to a decrease in crystallinity, while a lower polymer molecular weight facilitates fewer cross-linking sites, resulting in cracked surfaces. The

advantages in tunable 3D MXene-based aerogels' structural assemblies and high electronic conductivity have been exploited in many applications, including flexible electronics,<sup>137–140</sup> EMI shielding,<sup>141–147</sup> and energy-storage.<sup>148–151</sup> In the upcoming sections, we will elaborate on several MXene aerogel frameworks for functional applications.

### 3.3 | Bioinspired/biomimetic structures

Inspired by nature, several functional nanostructures have been fabricated by researchers to realize their performance in soft electronics, skin-inspired microelectronics, sensors, and actuators.<sup>117,152–156</sup> Among these, bioinspired nacre, leaf-like structures, and polymeric woods have been widely explored.<sup>157,158</sup> Especially, nacre-like structures induce exceptional mechanical reinforcing effects, thereby producing materials with high strength and stiffness. Such reinforcing effects can be realized from its intrinsic structural benefits in deliberately-designed “brick and mortar” assembly.


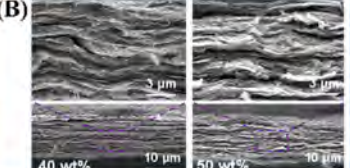
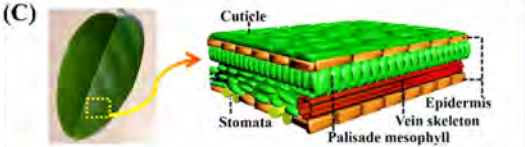

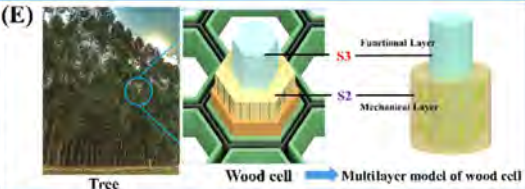
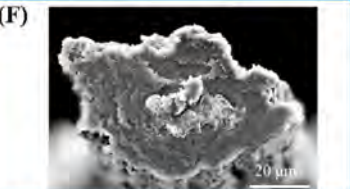
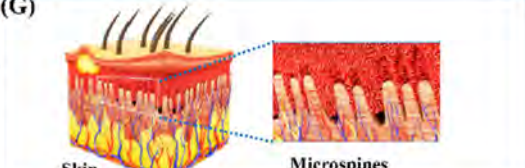
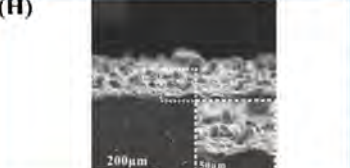


Scientists employed many approaches to mimic this structure utilizing various nanomaterials, including graphene,<sup>159–163</sup> MXene,<sup>164</sup> and nanoclay.<sup>165</sup>

Recently, 2D MXene-based bioinspired materials have shown promise in mimicking nacre-like nanocomposite structures and found extensive electronic applications in EMI shielding<sup>36,166,167</sup> and sensors.<sup>45,168</sup> In a recent study, Cao et al.<sup>35</sup> integrated d-Ti<sub>3</sub>C<sub>2</sub>T<sub>x</sub> MXene into cellulose nanofibers (CNFs) and produced a nacre-like layered composite paper via the process of vacuum-assisted filtration-assembly (Figure 4A). The nacre-like layered structure was confirmed by the cross-sectional morphology of the composite paper, revealing the function of 2D MXene as “brick” while 1D CNF displays the role of “mortar” (Figure 4B). The d-Ti<sub>3</sub>C<sub>2</sub>T<sub>x</sub>/CNF paper exhibited synergistic mechanical performance improvement, which originated from the biomimetic nacre structure. In that composite assembly, the 2D MXene

nanosheets as “bricks” formulated the frame of composite material. On the other hand, 1D CNFs bound MXene nanosheets tightly and facilitated stress transfer throughout structure, thus dissipating energy. Altogether, these synergistic reinforcing/toughening effects remarkably improved the strength and toughness of the paper, even higher than their parent constituents MXene and CNFs, individually. Although nacre-like structures are reported predominantly for mechanical reinforcing,<sup>170,171</sup> they have also enhanced EMI shielding performance. The above-mentioned composite paper also induced exceptional EMI shielding properties, which can be perceived from the nacre-like lamellar structure of d-Ti<sub>3</sub>C<sub>2</sub>T<sub>x</sub>/CNF as it endows multiple internal reflections. These resulted in the absorption and energy dissipation of the electromagnetic (EM) waves, ultimately exhibiting high EMI efficiency.

MXene-based structures also showed capability in mimicking leaf-like appearance for high-performance

	Natural prototype	Device morphology	Device features
Nacre	(A) 	(B) 	Tensile strength (~135.4 MPa), fracture strain (~16.7%), folding endurance (~14 260 times), electrical conductivity (~739.4 S m <sup>-1</sup> ) EMI shielding efficiency (~2647 dB cm <sup>2</sup> g <sup>-1</sup> ).
Leaf	(C) 	(D) 	The smart actuator depicts multi-responsiveness, fast actuation speed, low-power actuation, large-shape deformation, programmable adaptability and robust stability.
Wood polymer	(E) 	(F) 	Tensile strength (290 MPa), electrical conductivity (2400 S m <sup>-1</sup> ), temperature resistance (1800 S m <sup>-1</sup> with a reduction of about 30% at 100°C).
Microspine	(G) 	(H) 	High sensitivity (151.4 kPa <sup>-1</sup> ), response time less than 130 ms, subtle pressure detection limit of 4.4 Pa and cyclic stability over 10 000 cycles.

**FIGURE 4** (A) Schematic showing brick and mortar architecture in nacre; (B) SEM images illustrating a nacre-like compact lamellar structure in prepared d-Ti<sub>3</sub>C<sub>2</sub>T<sub>x</sub>/CNF composite paper. Reproduced with permission.<sup>35</sup> Copyright 2018, the American Chemical Society. (C) Photograph of natural leaf and schematic diagram of a leaf structure; (D) schematic diagram of the (MXCC/PC) bilayer-structured actuator. Reproduced with permission.<sup>169</sup> Copyright 2019, the American Association for the Advancement of Science. (E) The microstructure of the wood cell wall comprises of primary and three secondary layers (S1, S2, and S3), with the well-aligned cellulose microfibrils arranged in the S2 layer; (F) cross-sectional morphology of MXene/GO fibers. Reproduced with permission.<sup>152</sup> Copyright 2018, Royal Society of Chemistry. (G) Schematics of human-skin and microspines under the skin; (H) SEM images of microspiny MXene-based PDMS depicting the rough surface and side of the randomly distributed orientation. Reproduced with permission.<sup>45</sup> Copyright 2020, the American Chemical Society. CNF, cellulose nanofibers; EMI, electromagnetic interference; GO, graphene oxide; MXCC, MXene-cellulose; PC, polycarbonate; PDMS, polydimethylsiloxane

applications like programmable actuators and EMI shielding.<sup>88,169,172</sup> For example, a natural leaf-inspired smart actuation system has been developed by Cai et al.<sup>169</sup> First, a MXene-cellulose (MXCC) ink was produced by blending them homogeneously and then a bilayered MXCC and polycarbonate (PC) (MXCC/PC) was formulated by filtering MXCC ink on PC membrane. The obtained MXCC/PC membrane exhibited excellent efficiency in mimicking several important leaf microstructures. Typically, a leaf structure consists of a cuticle, epidermis, palisade mesophyll, vein skeleton, and stomata; all these structures in tandem allow the leaf to act as an effective photosynthetic medium<sup>173</sup> (Figure 4C,D). The MXCC/PC membrane has a design inspired from the leaf and several functions can be realized. For example, 2D MXene ( $\text{Ti}_3\text{C}_2\text{T}_x$ ) nanosheets mimic the palisade mesophyll structure and harvest electric or light energy and convert it to thermal energy. In contrast, the CNFs mimic the vein skeleton structure and enhance the robustness of the actuator while assisting in rapid shape change. In addition, PC mimics stomata and epidermis and displays the role of water insertion/extraction from the MXCC. The designed soft actuator demonstrated excellent responsiveness in response to different external stimuli, including humidity, electricity, and near-infrared (NIR) light. Such a nature-inspired smart actuator has tremendous potential to be employed in programmable soft devices.

Researchers mimicked the hierarchical layered wood structure<sup>152</sup> to design MXene-based fibers with a mechanical and functional support layer (Figure 4E). A biomimetic core-shell MXene/GO fiber was designed and fabricated by the co-axial wet spinning technique. The morphology of the hybrid fiber reveals that compared to a regular MXene/GO fiber, the core-shell MXene/GO fiber has a compact layered structure of MXene core and no void or gaps are noticeable as GO wraps the core effectively (Figure 4F). These structural assemblies benefit the fiber to have superior mechanical properties. In addition, the highly-conductive biomimetic fiber showed promise in EMI shielding. Cheng et al.<sup>45</sup> reported a MXene-based piezoresistive sensor emulating bioinspired microspinous microstructure for subtle pressure detection (Figure 4G). In this study, single-layer  $\text{Ti}_3\text{C}_2\text{T}_x$  was uniformly deposited on PDMS through a thermal spray-coating method. Scanning electron microscopy (SEM) imaging revealed that the MXene-based PDMS microstructure has a rough surface and randomly distributed microspines (Figure 4H). The sensor demonstrates great promise in several pressure-sensitive applications such as human-machine interactions and detection of human physiological signals.

### 3.4 | Printed structures

MXene undergoes uniform aqueous dispersion due to their hydrophilicity and highly negatively-charged MXene flakes with a Zeta potential of ca.  $-30$  mV, resulting in the rapid development of MXene-based printed devices. These characteristics of MXene also assist in forming a colloidal dispersion in various aqueous and organic solvents.<sup>20,174</sup> Also, recent developments in MXene ink showed promise in designing additive-free printed devices, which is considered a revolutionary approach in terms of environmental footprint when compared to other additive-mediated printing strategies.<sup>24</sup>

Several materials have been realized as an active material for printing such as carbon-based materials (1D CNT and 2D graphene), metallic nanoparticles, and conductive polymer-based inks.<sup>175,176</sup> Generally, graphene ink formulation is accomplished in NMP-based solvents. However, challenges associated with high boiling points and instability of active materials in NMP colloidal solutions significantly hinder their large-scale production.<sup>177</sup> Henceforth, researchers investigated several strategies to formulate inks that suppress the above-mentioned drawbacks by employing cosolvents, binders, or additives.<sup>8</sup> However, significant environmental concerns, postprocessing requirements, and marginal device functionality have discouraged researchers from using such additives. In Table 2, we summarize the pros and cons of different commonly used active material-based functional inks for printing electronic devices. Recently, additive-free MXene aqueous dispersions have been applied to design electronic devices by inkjet printing,<sup>178–182</sup> 3D printing,<sup>183–185</sup> and screen-printing.<sup>186,187</sup>

Additive-free MXene aqueous and organic inks were prepared by Zhang et al.,<sup>180</sup> by dispersing  $\text{Ti}_3\text{C}_2\text{T}_x$  nanosheets in water and several organic solvents such as DMF, DMSO, NMP, and ethanol, as demonstrated in Figure 5A. The inks were applied in inkjet and extrusion printing for microsupercapacitors (MSCs). It was found that the inverse Ohnesorge ( $Z$ ) numbers in the optimal range for stable inkjet printing requirements were ca. 2.6 for ethanol ink and ca. 2.2 for NMP ink. At an inkjet-printed line of 5, the electrical conductivity was as high as  $2770 \text{ S cm}^{-1}$  and maintained at  $510 \text{ S cm}^{-1}$  even after 6 months, while the printed lines exhibited a decrease in conductivity to  $1093 \text{ S cm}^{-1}$  after thousands of bending cycles. As shown in Figure 5B, a high-resolution printing pattern was observed without any coffee-ring effect using NMP and ethanol as the solvents. Moreover, for extrusion printing, MXene ink with a high concentration ( $\sim 36 \text{ mg mL}^{-1}$ ) and viscosity ( $\sim 0.7 \text{ Pa s}$ ) was employed, and the printed patterns (Figure 5C) demonstrated a dramatic decline in sheet resistance from 2000 to  $10 \text{ } \Omega \text{ sq}^{-1}$ . Significantly, both inkjet and extrusion printing were

**TABLE 2** Advantages and disadvantages of various nanomaterial enabled printed devices

Printing ink	Advantages	Disadvantages
2D MXene	<ul style="list-style-type: none"> <li>• High compatibility with different solution-based printing methods</li> <li>• High durability and tunable surface functionalities for the desired usage</li> <li>• Adhesives/additive-free printing opportunities</li> <li>• High stability in large concentration window (<math>1\text{--}100\text{ mg mL}^{-1}</math>)</li> <li>• Stable and tunable rheological behavior of MXene ink</li> <li>• Stable printed surfaces, and hence, no residual surfactants remain in printed surfaces after printing</li> <li>• Versatile fabrication, applications, and eco-friendly approach</li> </ul>	<ul style="list-style-type: none"> <li>• Being nascent in research, improving MXene ink stability and rheological properties are yet to fully understand</li> <li>• Challenge in the synthesis of uniform surface terminations for MXenes and ink formulation</li> <li>• Lacks industry viable and scalable opportunity</li> <li>• Cost concern and translational research facilities</li> <li>• Device integration and realizing new multifunctional usage purpose</li> </ul>
2D graphene	<ul style="list-style-type: none"> <li>• Excellent rheological behavior</li> <li>• Durability over mechanical deformations</li> <li>• High electrical conductivity</li> <li>• Highly suitable for additive printing manufacturing techniques</li> <li>• High controllability of print resolution</li> <li>• Widely accessible to various printing methods</li> <li>• Versatility in device fabrication and applications</li> </ul>	<ul style="list-style-type: none"> <li>• Instability in colloidal solution</li> <li>• Require postprocessing to remove surfactants</li> <li>• Require low viscosity inks</li> <li>• Limited control of pattern size and edge of pattern</li> <li>• Scalable production and cost concern</li> </ul>
Metal nanoparticle	<ul style="list-style-type: none"> <li>• Easy to dissolve and apply</li> <li>• Highly conductive</li> <li>• Versatile patterns and applications</li> </ul>	<ul style="list-style-type: none"> <li>• Susceptible to skin inflammation</li> <li>• Has sedimentation issues due to dispersion instability</li> </ul>

implemented in MSCs formation and offered excellent electrochemical performance.

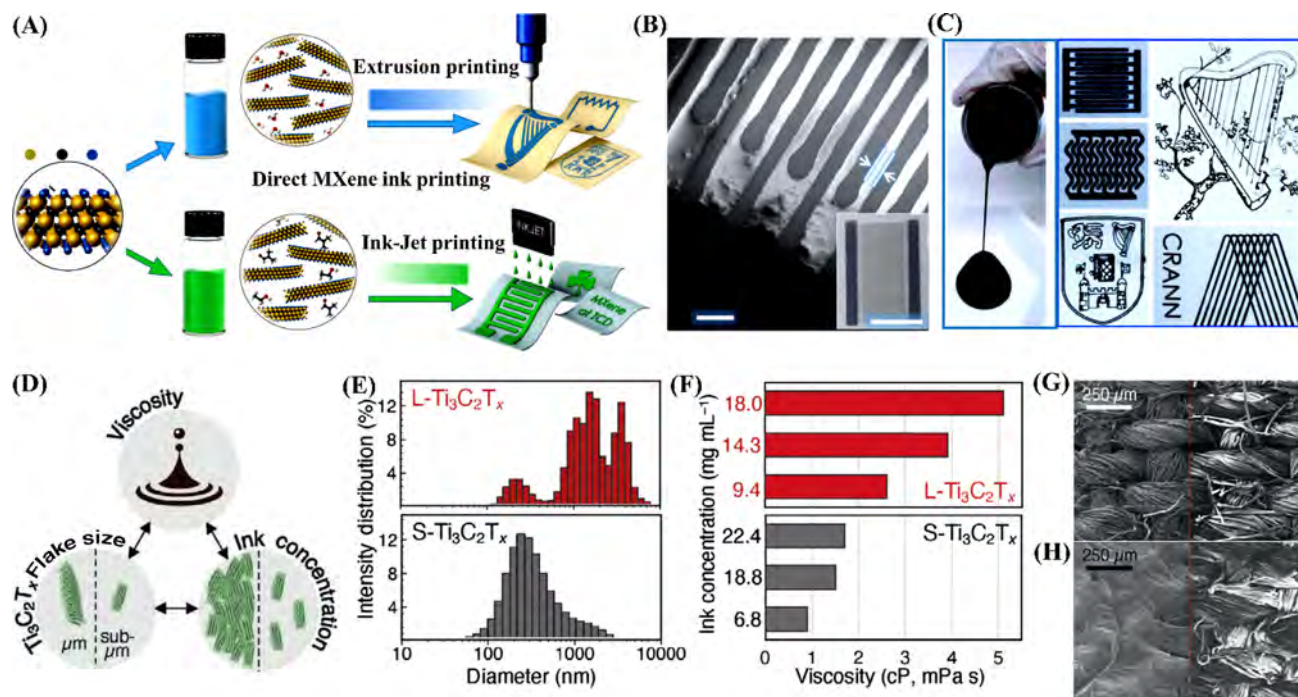
MXene nanosheets were doped with nitrogen by a melamine-formaldehyde method to formulate an ink for extrusion-based 3D printing, to take advantage of enhanced reinforcing effect on conductivity and electrochemical reactivity of crumpled nitrogen (N).<sup>187</sup> The N-doped MXene was mixed with activated carbon (AC), CNTs, and GO to adjust the viscosity of the ink system and eliminate additional binders for 3D printing. The ink showed excellent shear thinning behavior, which enabled the ink to be 3D printed efficiently without any clogging during extrusion. Further rheological study revealed that the as-prepared ink could maintain stable 3D structural assemblies while printing.

Furthermore, Uzun et al.<sup>178</sup> applied MXene ink into inkjet-printed textile substrates. The viscosity of the additive-free  $\text{Ti}_3\text{C}_2\text{T}_x$  MXene ink can be modulated by controlling the  $\text{Ti}_3\text{C}_2\text{T}_x$  flake size and concentration (Figure 5D). Both large ( $\text{L-Ti}_3\text{C}_2\text{T}_x$ ) and small ( $\text{S-Ti}_3\text{C}_2\text{T}_x$ ) MXene flakes with submicron (average lateral size of 350 nm) and micron (average lateral size of 2  $\mu\text{m}$ ) sizes ink with different concentrations were utilized in

printing lines (Figure 5E). It was revealed that the more significant decrease in sheet resistance with larger flakes compared to the small ones could be due to the disruptions in internal contact of  $\text{S-Ti}_3\text{C}_2\text{T}_x$  nanosheets. Moreover, with the above-mentioned average flake sizes for both  $\text{S-Ti}_3\text{C}_2\text{T}_x$  and  $\text{L-Ti}_3\text{C}_2\text{T}_x$ , the viscosity was  $\sim 1.5\text{ cP}$  at  $18.8\text{ mg mL}^{-1}$  and  $5.1\text{ cP}$  at  $18.0\text{ mg mL}^{-1}$ , respectively (Figure 5F). As observed from the SEM images, the fabrics printed with  $\text{L-Ti}_3\text{C}_2\text{T}_x$  demonstrated significant growth of  $\text{Ti}_3\text{C}_2\text{T}_x$  film on the fabric surfaces with the successive number of print passes from 1 to 10 (Figure 5G,H). Finally, benefiting from the fragmented structure of  $\text{S-Ti}_3\text{C}_2\text{T}_x$  flakes that provide access to ion for electrode layer and the high conductive nature of  $\text{L-Ti}_3\text{C}_2\text{T}_x$  flakes, a textile-based MSC was fabricated. The electrochemical performance of the MSC was found to be higher by two orders of magnitude compared to other printed textile-based MSCs.

The unique rheological behavior and tunable viscosity of MXene inks facilitate processing the inks for screen printing. For instance, Abdolhosseinzadeh et al.<sup>188</sup> implemented a sustainable “turning trash into treasure” strategy to formulate MXene ink without additives. The unetched MAX phase and unexfoliated sediments are





**FIGURE 5** (A) MXene-enabled extrusion and ink-jet processes for device fabrication; (B) SEM image of the inkjet-printed microsupercapacitor employing the NMP ink. Inset showing the full device, (C) demonstration of viscous nature of MXene aqueous ink, and the optical images of all-MXene various printed patterns with different designs. Reproduced with permission.<sup>180</sup> Copyright 2019, Springer Nature. (D) Three essentials of aqueous  $\text{Ti}_3\text{C}_2\text{T}_x$  MXene ink formulation: viscosity,  $\text{Ti}_3\text{C}_2\text{T}_x$  flake size, and  $\text{Ti}_3\text{C}_2\text{T}_x$  concentration. (E) Effect of large and small flake size distribution MXene inks. (F) Plot of viscosity versus ink concentration at large and small flake sizes; and (G, H) SEM images of large flake size woven fabrics at 1 and 10 print pass. The left side of the dashed line showing the  $\text{Ti}_3\text{C}_2\text{T}_x$ -printed part and the right side presents neatly woven fabric. Reproduced with permission.<sup>178</sup> Copyright 2020, WILEY-VCH Verlag. NMP, *N*-methyl-2-pyrrolidone; SEM, scanning electron microscopy

collected by separating supernatants (few-layered  $\text{Ti}_3\text{C}_2\text{T}_x$  nanosheets) during sonication and centrifugation. A small percentage of delaminated MXene ( $\text{d-Ti}_3\text{C}_2\text{T}_x$ ) nanosheets remained in the decanting supernatant solution to form sediment ink by a three-roll mill process, where  $\text{d-Ti}_3\text{C}_2\text{T}_x$  offered mechanical integrity and electrical conductivity. The ink exhibited a shear-thinning behavior and non-Newtonian properties along with a viscosity of 35 Pa s. Finally, the high resolution and uniform printing spatiality allowed the ink to screenprint on various substrates.

## 4 | EMERGING APPLICATIONS IN FLEXIBLE AND WEARABLE ELECTRONICS

### 4.1 | Energy storage and harvesting

The current advancement in powering portable and flexible electronic devices has been revolutionized by the tremendous development of lightweight, flexible, and

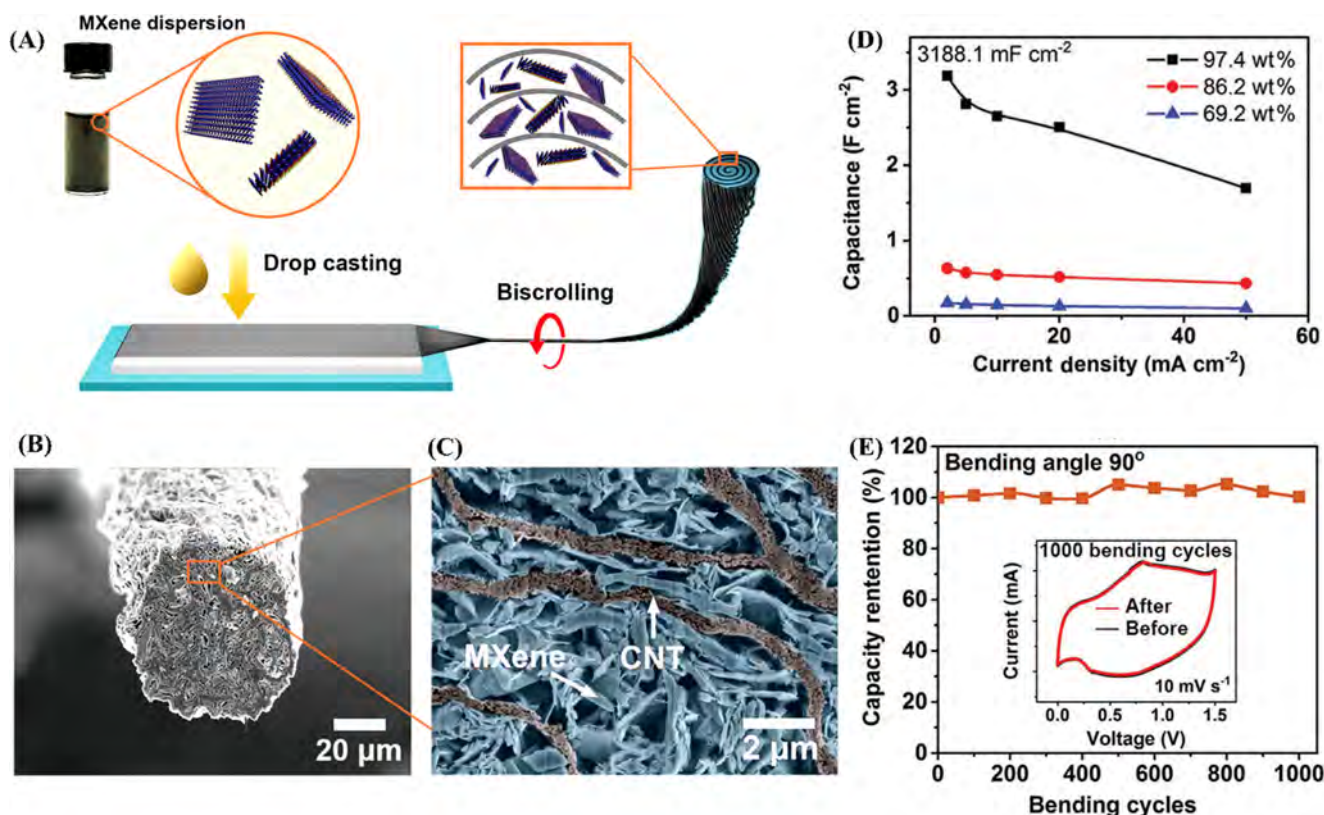
wearable energy storage platforms. In contrast to conventional batteries and capacitors, supercapacitors are rewarding in terms of high-performance devices coupled with high rate capacity, charge storing capability, flexibility and stretchability, stable charge–discharge performance and long cyclic life expectancy.<sup>15,189–191</sup> Like graphene, MXenes endow exceptional energy-storing ability due to their outstanding electrical conductivity, tunable surface terminations, high surface area, and peculiar geometry in structure.<sup>192,193</sup>

Textiles or fiber-shaped SCs can be particularly useful in powering wearable electronics because of their low weight, comfort, flexibility, and enhanced electrode performance. Enormous progress has been seen in MXene fibers/yarns or woven/knitted fabric-based electrodes prepared from a wide variety of techniques.<sup>15,82</sup> Researchers have reported a novel smart-textile composite electrode manufactured from the conformal coating of MXene onto textile substrates. Using electrospinning and wet spinning approaches, novel and core-shell fibers can also be manufactured for smart-electrode systems.<sup>194</sup> In the electrode formation, fiber or textile-shaped

supercapacitors are required to possess efficient charge storage/transportation facilities, high electrical conductivity, porosity, excellent redox reaction or intercalation ability, and above all, fibers or yarns should have sufficient strength to withstand the stresses of different knitting or weaving forces/tensions.<sup>195</sup> Besides, the ideal surface chemistry of MXene, such as appropriate flake size, plays a vital role in designing textile-based electrode materials. When assembled as SCs these devices exhibit enhanced power and energy densities, volumetric, areal, gravimetric capacitance, and long cycle stability. For instance, an electrospun MXene (90 wt%) loaded MXene/rGO composite fiber electrode depicted excellent volumetric ( $890.7 \text{ F cm}^{-3}$ ), areal ( $565.4 \text{ mF cm}^{-2}$ ), and gravimetric ( $494.8 \text{ F g}^{-1}$ ) capacitance. In that hybrid fiber structure, the well-aligned MXene nanosheets inside the hybrid fibers and the synergistic effects of MXene and liquid crystal ability of GO are responsible for the electrochemical performance of the fiber electrode.<sup>196</sup> Several similar electrodes developed from MXene/rGO systems have also been reported as high-performance SCs.<sup>99,148,150</sup>

Biscrolling is the technique where a twist is inserted in a host sheet that is overlaid with the guest material.<sup>197</sup>

Two-dimensional MXene nanosheets have also been incorporated with 1D CNTs by biscrolling techniques to prepare yarn electrodes, achieving a high MXene content ( $\sim 98 \text{ wt}\%$ ).<sup>198</sup> The as-obtained electrode demonstrated superior electrochemical performances along with high capacitance retention ability.<sup>199,200</sup> Wang et al.<sup>198</sup> designed a yarn-shaped flexible SC by biscrolling MXene with CNTs (BMX; Figure 6A). As evident from the cross-sectional images of the highly MXene-loaded BMX yarn that MXene nanosheets are entrapped within the CNT yarn corridors (Figure 6B,C). When assembled as free-standing SCs, the BMX yarn delivered excellent specific volumetric ( $1083 \text{ F cm}^{-3}$ ), aerial ( $3188 \text{ mF cm}^{-2}$ ), gravimetric ( $428 \text{ F g}^{-1}$ ), and linear capacitance ( $118 \text{ mF cm}^{-1}$ ) at a current density of  $2 \text{ mA cm}^{-2}$ , and excellent capacitance retention under different bending conditions<sup>198</sup> (Figure 6D,E). Additionally, the developed energy textile was demonstrated to power a digital timer for over 10 min. It is also possible to develop neat MXene fibers directly from the wet-spinning technique, offering a volumetric capacitance of  $1265 \text{ F cm}^{-3}$  with virtually complete capacitance retention even after 10 000 cycles.<sup>83</sup> Overall, MXene-mediated textiles have provided outstanding opportunities in fiber/yarn-shaped wearable



**FIGURE 6** (A) Fabrication process of BMX yarn; (B) cross-sectional morphology of the BMX yarn with 97.4 wt% MXene content; (C) magnified color SEM image of the indicated section in (D) specific areal capacitance of the BMX yarn electrodes, (E) cycle stability before and after different bending angles and cycles. Reproduced with permission.<sup>198</sup> Copyright 2018, WILEY-VCH Verlag. BMX, biscrolling MXene; CNT, carbon nanotube; SEM, scanning electron microscopy

SCs, and more possible avenues can be explored in recent literature.<sup>87,201</sup>

Electrodes with excellent unique 3D macroscopic porous architectures have shown promise in supercapacitors, owing to their superior electrolyte permeabilities and rapid electron/ion transports in the electrode system.<sup>31</sup> Hydrogels are such materials with 3D structure, and have been utilized in SCs. MXene-derived hydrogels are the intriguing choice for SCs as they provide excellent conductive networks and ion diffusion pathways, as well as delivering high electrode attributes. As such, by employing a one-step hydrothermal method, Zhang et al.<sup>128</sup> manufactured an MXene assisted self-assembled laminar-structured GO 3D hydrogel electrode for SCs. The hybrid hydrogel had a large specific surface area of  $161.1 \text{ m}^2 \text{ g}^{-1}$  and a high pore volume of  $0.5 \text{ cm}^3 \text{ g}^{-1}$ , and facilitated high energy densities (9.3 and  $5.7 \text{ Wh kg}^{-1}$ ), at different power densities of 500 and  $5000 \text{ W kg}^{-1}$  when configured symmetrically. Furthermore, perfect capacitance retention was achieved after 10 000 continuous charge–discharge cycles. MXene also shows promise as a building block for hydrogel formation with 1D polypyrrole nanofibers and PVA matrix.<sup>202</sup> The assembled 3D hydrogel system led to excellent enhancement of mechanical robustness and demonstrated prominence in wearable SC applications. In another study, MXene-rGO aerogel-based mechanically robust self-healable 3D MSC was fabricated using an ice template method and was wrapped by a self-healing polyurethane shell for self-healing.<sup>150</sup> The aerogel MSC accomplished outstanding electrochemical characteristics such as high area-specific capacitance of  $34.6 \text{ mF cm}^{-2}$  at a scan rate of  $1 \text{ mV s}^{-1}$  and excellent cycling stability with capacitance retention of up to 91% over 15 000 cycles. Lately, several MXene aerogel electrode systems have been reported for enhanced electrochemical performances of supercapacitors.<sup>148,151</sup>

MXene-printed structures have also emerged as desirable options for designing MSC electrodes with high electrochemical properties.<sup>174</sup> Li et al.<sup>203</sup> reported a screen-printed MSC electrode by taking an in situ process thus uniformly anchoring hydrous ruthenium oxide ( $\text{RuO}_2$ ) nanoparticles on as-synthesized  $\text{Ti}_3\text{C}_2\text{T}_x$  MXene nanosheets (Figure 7A–C). Silver nanowires (AgNWs) were utilized to endow high viscosity and suitable rheological behavior for the electrode ink and also precluded additives. The produced MSCs demonstrated superior volumetric capacitance of  $864.2 \text{ F cm}^{-3}$  at a scan rate of  $1 \text{ mV s}^{-1}$ , high rate capacity ( $\sim 2000 \text{ mV s}^{-1}$ ), excellent cycle stability (90% retention after 10 000 cycles), and excellent flexibility (87.3% retention after 2000 bending cycles; Figure 7D–F). Other printing methods also demonstrated feasibility in printing electronic devices. For example, an additive-free nitrogen-doped MXene ink was formulated to print SCs via an extrusion-

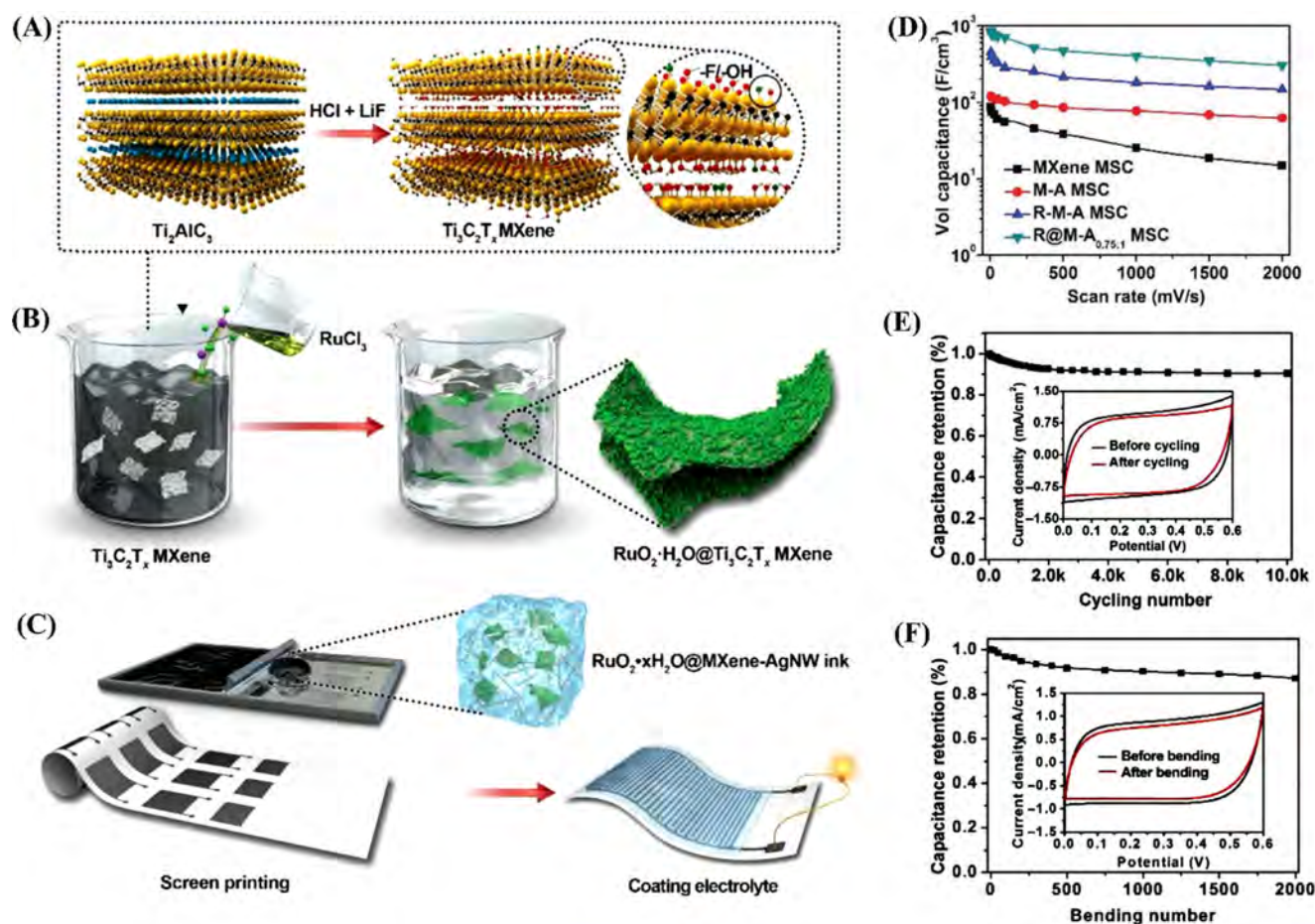
based 3D printing.<sup>180</sup> The printed device features a high areal and volumetric energy density of  $0.42 \text{ mWh cm}^{-2}$  and  $0.83 \text{ mWh cm}^{-3}$ , respectively, when assembled as an asymmetric supercapacitor system.<sup>187</sup> Likewise, 3D printing was used to print various objects with a high specific surface area and showed improved electrochemical properties along with superior cycle stability.<sup>204</sup> The electrochemical performances of various MXene architectural devices are summarized (Table 3).

Triboelectric nanogenerators (TENGs) have been regarded as a small-volume, low-cost, human-friendly, and effective means of harvesting energy.<sup>206–208</sup> Inspired by several dynamic human biomechanical motions, TENGs are utilized to convert kinetic energy to electricity and are formulated via coupling triboelectrification and electrostatic induction between different materials. In TENGs, the electrification and charge transfer occur based on contact-separation, sliding, or friction between two dissimilar materials such as polymers and metals, depending on the electrostatic induction and triboelectric series.<sup>209</sup> MXenes are advantageous for TENG applications due to the enhanced dielectric constants that emerge from functional fluorine and oxygen groups. In addition, the 2D structure of MXene accumulates charge between interlayer sheets and the polymer matrix.<sup>207</sup> MXenes can improve the TENG performance by enhancing the electronegativity and electrical conductivity of the materials.<sup>210</sup> A fabric-based TENG developed by Xiong et al.<sup>211</sup> showed potential in harvesting energy from water flow, whereas, the TENG performance was greatly influenced by the water molecules adhered with the device surface, preventing its efficient-energy harvesting abilities. Therefore, researchers designed a hydrophobic fabric-based MXene/Ecoflex nanocomposite TENG system inspired by several human biomechanical motions and environmental situations.<sup>209</sup> The developed TENG offered a maximum output peak power of 3.69 mW and a power density of  $9.24 \text{ W m}^{-2}$ . Cao et al.<sup>210</sup> integrated liquid MXene, CNFs, and soft silicon rubber to develop a shape-adaptable TENG for a self-powered biomechanical sensor. In this TENG system, CNFs functioned as a dispersant and interlocking agent for ensuring an effective interconnected network of MXene, while silicone rubber acted as a packaging and triboelectrification layer. This TENG could harvest energy and showed potential to power several electronic systems, including real-time monitoring of various human motions.<sup>210</sup>

## 4.2 | Wearable health monitoring

The human body generates various physiological signals such as muscle movement, electrocardiogram (ECG),





**FIGURE 7** Schematic representation of (A) the synthesis procedure of  $\text{Ti}_3\text{C}_2\text{T}_x$  MXene; (B) synthesis techniques of  $\text{RuO}_2 \cdot x\text{H}_2\text{O}@\text{MXene}$  nanocomposite; (C) formation of screen-printed flexible MSC devices; (D) volumetric capacitance at different scan rates of various MXene MSCs; (E) cycling stability at a scan rate of  $100 \text{ mV s}^{-1}$  (inset showing CV curves before and after cycling); and (F) cycle stability at different bending cycles to a bending strain of 5.0% (inset showing CV curves taken at  $100 \text{ mV s}^{-1}$  before and after 2000 bending cycles). Reproduced with permission.<sup>203</sup> Copyright 2019, WILEY-VCH Verlag. CV, cyclic voltammetry; MSC, microsupercapacitor;  $\text{RuO}_2$ , ruthenium oxide

skin temperature, blood pressure, wrist pulse, breath/heart rate, etc., which contain critical health information. Wearable electronic (e)-skins can deliver physiological information by placing the sensor conformally over human skin. The information provided is transmitted to a microcontroller for signal interpretation and continuous health surveillance.<sup>212,213</sup>

MXene-based wearable e-skins have been widely used for healthcare applications, such as voice recognition and the monitoring of blood pressure, heart pulse, muscle movement, and facial expression.<sup>214–216</sup> Recently, Sharma and co-workers<sup>217</sup> reported an MXene composite nanofibrous mat-based capacitive pressure sensor for reliable monitoring of physiological signals (Figure 8A). The sensitivity of the device was increased by a factor of five because of the higher dielectric constant of MXene and the decrease in the compression modulus of the scaffold. The MXene nanofibrous-based sensor showed a distinct pulse waveform from the radial artery, including P-wave,

T-wave, and D-wave (Figure 8B,C), which provide information on arterial stiffness and vascular health an early stage detection of Parkinson's disease (Figure 8D,E). Wang and co-workers<sup>116</sup> developed a modified MXene composite stretchable hydrogel for wearable bioelectronics. MXene was used as a base nanomaterial in hydrogel to enhance conductivity and improve polymerization and cross-linking of the polymer chains. The electrical signal from the ECG, electrooculography (EOG), and electromyogram (EMG) provides vital information on the heart, ocular condition, muscle contraction, and relaxation status, respectively (Figure 8F–J), which are valuable for predicting various illnesses such as musculoskeletal disorders, heart attack, sleep apnea, etc. The high conformity of the self-adhesive MXene-based hydrogel offered a lower contact impedance and a high signal-to-noise ratio.

Song et al.<sup>218</sup> fabricated an MXene/PDMS composite piezoresistive pressure sensor for large deformation monitoring. MXene was coated on a porous PDMS scaffold,

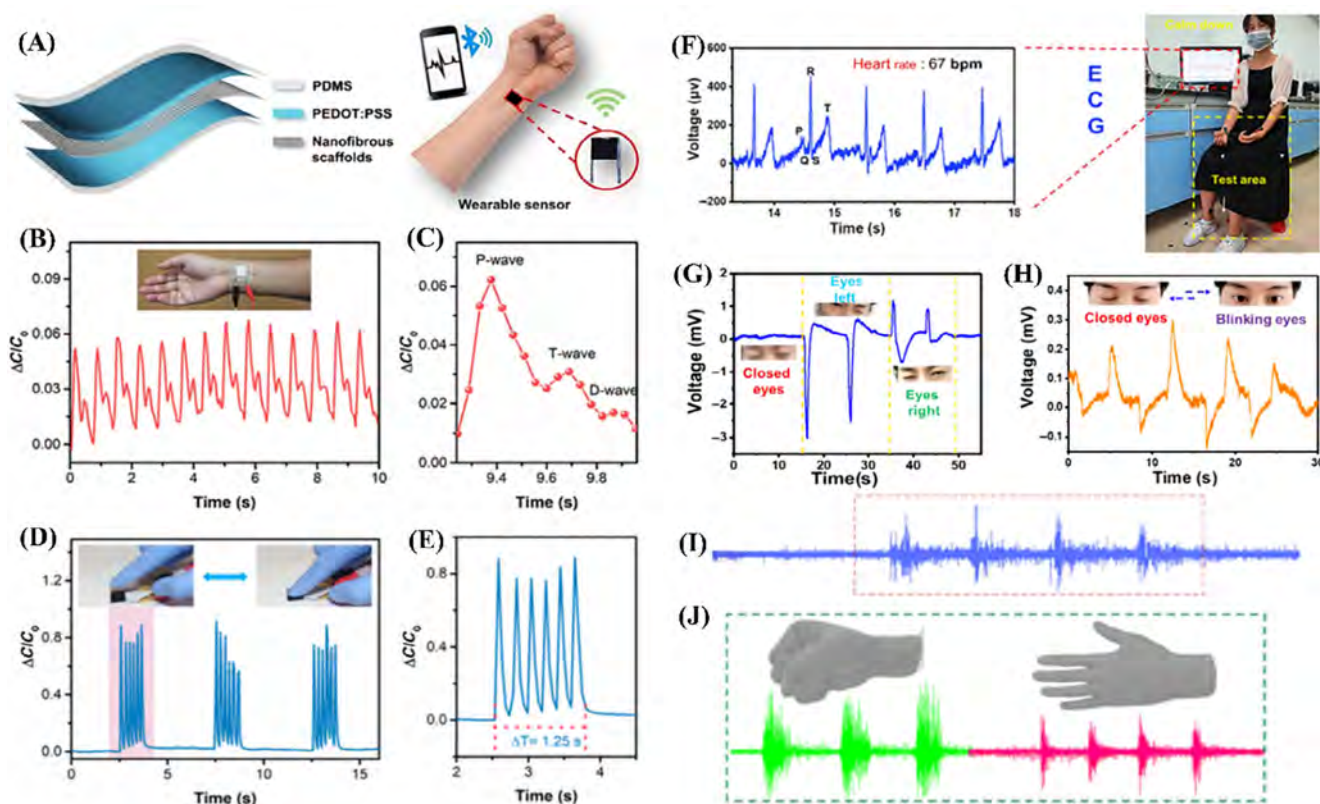
and the sensor successfully measured facial muscle movement, knee bending, finger-bending with different speeds, and swallowing process. Impressively, the

synergistic effect of MXene composite has also been investigated for biomedical applications because of its superior electrical, mechanical, and chemical properties.

**TABLE 3** Summary of the electrochemical performances of various MXene-based nanostructure devices

Electrode materials	Device design	Electrolyte	Energy storage parameters	Capacitance retention	Ref
Ti <sub>3</sub> C <sub>2</sub> T <sub>x</sub> /rGO fiber	Textile	PVA/H <sub>2</sub> SO <sub>4</sub>	The areal capacitance of 550.96 mF cm <sup>-2</sup> , gravimetric capacitance of 110.89 F g <sup>-1</sup>	85% @ 10 000th cycle	205
Ti <sub>3</sub> C <sub>2</sub> T <sub>x</sub> /PEDOT:PSS fiber	Textile	1 M H <sub>2</sub> SO <sub>4</sub>	Areal capacitance of 676 mF cm <sup>-2</sup> , gravimetric capacitance of 258 F g <sup>-1</sup> , volumetric capacitance of 615 F cm <sup>-3</sup>	~95% @ 10 000th cycle	100
Ti <sub>3</sub> C <sub>2</sub> T <sub>x</sub> /rGO fiber	Textile	1 M H <sub>2</sub> SO <sub>4</sub>	Areal capacitance of 233 mF cm <sup>-2</sup> , gravimetric capacitance of 257 F g <sup>-1</sup> , volumetric capacitance of 341 F cm <sup>-3</sup>		99
Biscrolled MXene/CNT yarn	Textile	3 M H <sub>2</sub> SO <sub>4</sub>	Areal capacitance of 3188 mF cm <sup>-2</sup> , gravimetric capacitance of 523 F g <sup>-1</sup> , volumetric capacitance of 1083 F cm <sup>-3</sup>	~90% @ 10 000th cycle	198
Ti <sub>3</sub> C <sub>2</sub> T <sub>x</sub> -coated cellulose yarn	Textile	1 M H <sub>2</sub> SO <sub>4</sub>	Areal capacitance of 3965 mF cm <sup>-2</sup> , volumetric capacitance of 0.26 F cm <sup>-3</sup>	100% @ 10 000th cycle	102
Ti <sub>3</sub> C <sub>2</sub> T <sub>x</sub> -coated carbon fabric	Textile	1 M H <sub>2</sub> SO <sub>4</sub>	Areal capacitance of 416 mF cm <sup>-2</sup> , gravimetric capacitance of 200 F g <sup>-1</sup>	98% @ 20 000th cycle	86
Ti <sub>3</sub> C <sub>2</sub> T <sub>x</sub> -coated cotton knit fabric	Textile	1 M H <sub>3</sub> PO <sub>4</sub>	Areal capacitance of 707 mF cm <sup>-2</sup> , gravimetric capacitance of 31 F g <sup>-1</sup>	100% @ 10 000th cycle	81
Ti <sub>3</sub> C <sub>2</sub> T <sub>x</sub>	Hydrogel	3 M H <sub>2</sub> SO <sub>4</sub>	Gravimetric capacitance of ~226 F g <sup>-1</sup>	97.1% @ 10 000th cycle	133
Ti <sub>3</sub> C <sub>2</sub> T <sub>x</sub>	Hydrogel	Ionic liquid	Gravimetric capacitance of 70 F g <sup>-1</sup>	80% @ 1000th cycle	119
Ti <sub>3</sub> C <sub>2</sub> T <sub>x</sub> /PPy	Hydrogel	PVA/H <sub>2</sub> SO <sub>4</sub>	Gravimetric capacitance of 614 F g <sup>-1</sup>	100% @ 10 000th cycle	202
Ti <sub>3</sub> C <sub>2</sub> T <sub>x</sub> /rGO	Aerogel	2 M ZnSO <sub>4</sub>	Gravimetric capacitance of 128.6 F g <sup>-1</sup>	95% @ 75 000th cycle	148
Ti <sub>3</sub> C <sub>2</sub> T <sub>x</sub> /rGO	Aerogel	PVA/H <sub>2</sub> SO <sub>4</sub>	Areal capacitance of 34.6 mF cm <sup>-2</sup>	91% @ 15 000th cycle	150
Ti <sub>3</sub> C <sub>2</sub> T <sub>x</sub>	3D printed	PVA/H <sub>2</sub> SO <sub>4</sub>	Areal capacitance of ~1035 mF cm <sup>-2</sup> , areal energy density of 51.7 μWh cm <sup>-2</sup>		204
Ti <sub>3</sub> C <sub>2</sub> T <sub>x</sub>	3D printed	PVA/H <sub>2</sub> SO <sub>4</sub>	Gravimetric capacitance of 242.5 F g <sup>-1</sup>	90% @ 10 000th cycle	185
Ti <sub>3</sub> C <sub>2</sub> T <sub>x</sub>	Screen/extrusion printed	PVA/H <sub>2</sub> SO <sub>4</sub>	Areal capacitance of 70.1 mF cm <sup>-2</sup>	92% @ 7000th cycle	187
Ti <sub>3</sub> C <sub>2</sub> T <sub>x</sub> and Co-Al LDH	Screen printing	PVA/KOH	Areal capacitance of 28.5 F cm <sup>-2</sup> , areal energy density 8.84 μWh cm <sup>-2</sup> , power density 230 μW cm <sup>-2</sup>	92% @ 10 000th cycle	186
Ti <sub>3</sub> C <sub>2</sub> T <sub>x</sub>	Inkjet printed	PVA/H <sub>2</sub> SO <sub>4</sub>	Areal capacitance of 294 mF cm <sup>-2</sup>	100% @ 10 000th cycle	178
Ti <sub>3</sub> C <sub>2</sub> T <sub>x</sub> /sodium ascorbate	Inkjet printed	PVA/H <sub>2</sub> SO <sub>4</sub>	Areal capacitance of 108.1 mF cm <sup>-2</sup> , volumetric capacitance of 720.7 F cm <sup>-3</sup>	-	182
RuO <sub>2</sub> ·xH <sub>2</sub> O@ Ti <sub>3</sub> C <sub>2</sub> T <sub>x</sub> -Ag NWs	Inkjet printed	PVA/KOH	Volumetric capacitance of 864.2 F cm <sup>-3</sup> , volumetric energy density of 13.5 mWh cm <sup>-3</sup> at power density of 48.5 W cm <sup>-3</sup>	90% @ 10 000th cycle	203

Abbreviations: CNT, carbon nanotubes; NWs, nanowires; PEDOT, PSS, poly(3,4-ethylenedioxythiophene) polystyrene sulfonate; PPy, polypyrrole; PVA, polyvinyl alcohol; rGO, reduced graphene oxide; RuO<sub>2</sub>, ruthenium oxide.



**FIGURE 8** (A) Schematic showing MXene nanofibrous-based pressure sensor; (B) monitoring of the radial artery pulse wave. Inset image showing the sensor attached to the wrist's dermal area; (C) extended image and detailed characteristic peaks of a single pulse waveform; (D) demonstration of sensors ability to emulating finger knocking for early detection of Parkinson's disease. Inset showing photograph of mimicked finger knocking on the sensor surface; (E) magnified image showing of emulated tapping. Reproduced with permission.<sup>217</sup> Copyright 2020, the American Chemical Society. (F) Real-time monitoring of ECG and heart rate of a girl resting in a quiet room by as prepared  $\text{TiO}_2/\text{MXene}$ -PAA hydrogel bioelectrodes; (G, H) eye movement monitoring by the hydrogel bioelectrode; (I, J) various voltage potential specific patterns obtained by various hand gestures. Reproduced with permission.<sup>116</sup> Copyright 2020, Elsevier. ECG, electrocardiogram; PAAm, polyacrylamide; PEDOT, PSS, poly(3,4-ethylenedioxythiophene) polystyrene sulfonate; PDMS, polydimethylsiloxane

Furthermore, Bi et al.<sup>138</sup> and Zhu et al.<sup>137</sup> fabricated AgNWs/MXene and graphene/MXene piezoresistive aerogels, for ultrasensitive e-skin. MXene composite aerogels facilitated a directional freezing strategy and superior tunable conductive pathway for operation in a broad application for flexible electronics. The application of the sensor for the recognition of various body deformations (ankle and wrist bending, cheek bulging, and throat swallowing) has been successfully demonstrated, useful for the rehabilitation of older populations. In addition, Pu and co-workers<sup>93</sup> have developed multilayered MXene/AgNWs smart composite fabrics for monitoring, analyzing, and correcting postures for medical applications. MXene was used effectively to improve the crack propagation mechanism, which in turn offered high-stress sensitivity. Intelligent composite fabrics offer excellent surveillance of human postures (head forward, shoulder imbalance, and kyphosis). Real-time monitoring of these postures helps minimize future complications such as shoulder pain, back pain, neck stiffness, etc.

### 4.3 | Wearable sensors for human-machine interactions

Motion sensors can convert the stress or tension generated by body deformations into an electrical signal.<sup>219–221</sup> The electrical signal can be used to control various machines, using the interface of human-machine interaction. Numerous wearable pressure and strain sensors have been used to control robotic arms and toy vehicles, etc., through body movements after integrating with microcontrollers and wireless modules.<sup>219,222–225</sup>

MXene-impregnated biodegradable tissue paper can be used as a wearable wide range HMI device (Figure 9A).<sup>226</sup> The MXene hydrophilic nanosheets adhere firmly to the surface of the highly-porous fabric, allowing a distinct conductive path under different deformation patterns. Recently, Zhang and co-workers<sup>118</sup> reported an MXene hydrogel-based strain sensor. Because of the excellent interconnection and improved H-bonding offered by MXene nanosheets, the hydrogel showed a remarkable



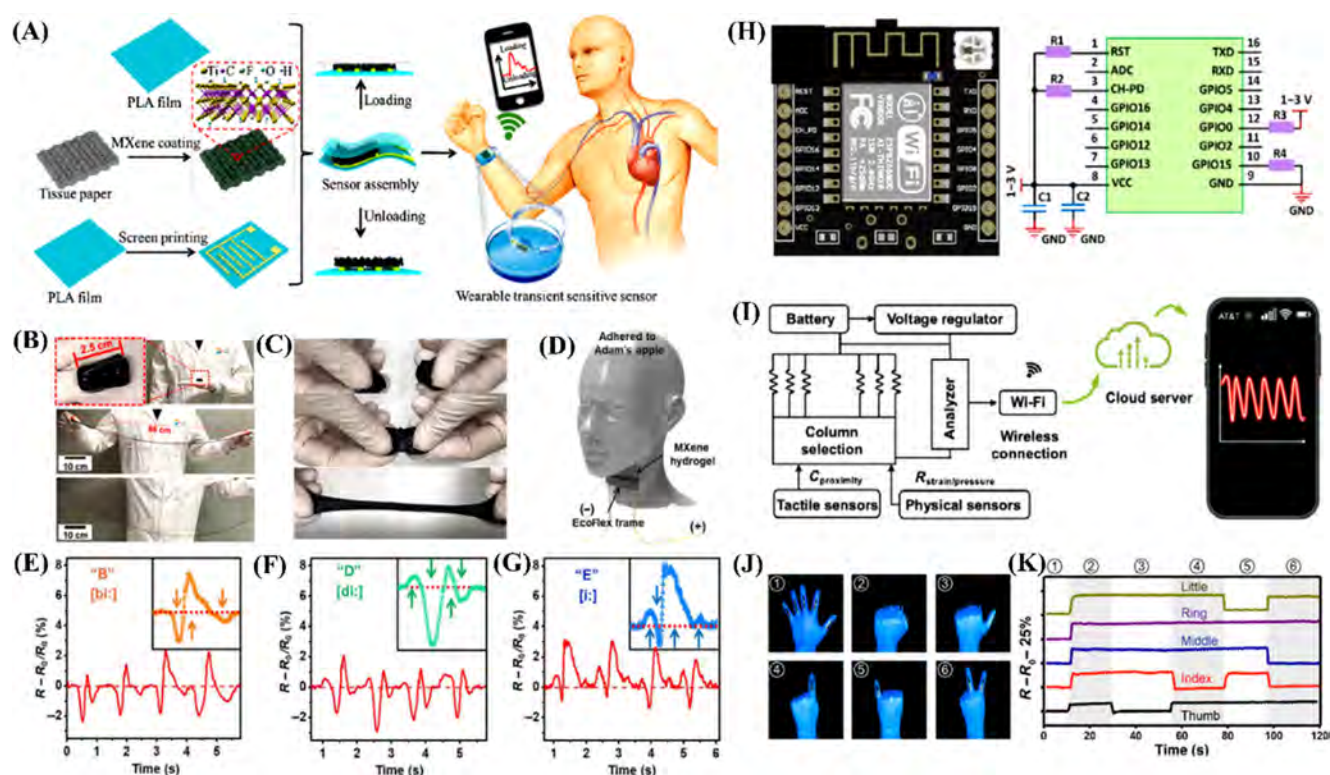
stretchability of more than 3400% (Figure 9B,C).<sup>118</sup> The highly-sensitive hydrogel was mounted on the throat at the larynx to detect sound vibration in the form of an electrical signal (Figure 9D–G). The detected signal was converted to the corresponding working voltage to enable control of the machinery by voice command. Furthermore, MXene hydrogel heterostructure e-skin can be used as a motion sensor, as shown in Figure 9H–K, where two MXene hydrogels were separated by a dielectric layer to induce a capacitive effect for applied deformations.<sup>117</sup> The hydrogel perfectly perceives different finger movements and generates distinct patterns, which can be synchronized via a wireless module to control equipment and machinery. The robotic arms can perfectly mimic the movement of the human finger, showing the excellent feasibility of a human–machine interface system.

#### 4.4 | EMI shielding

Marked by the unprecedented advances in miniaturized electronic technology, consumption of electronic and

smart gadgets experienced exponential growth in the 20th century. As a result, these devices continuously exert EM rays, which could be very detrimental to human health and the modern warfare system.<sup>227</sup> Significant measures, materials, and devices have been developed to minimize or protect electronic devices from EM waves. The newly-emerged 2D MXene brings about exceptional improvement in designing EMI shielding materials that can be ascribed to their superior features in terms of electrical conductivity, enriched and tailorable surface functionalities, large specific surface area, and being lightweight.<sup>135,142,143,147,181</sup> Altogether, these structural synergistic features lead to the fabrication of MXene-functionalized multifaceted architectures, namely nanocomposite films, smart-textiles, 3D hydrogels and aerogels, and printed substrates for EMI shielding.

Bioinspired nacre architectures promote efficient and multiple internal reflection pathways; thus attenuates incident EM waves. In MXene-mediated nacre-inspired structures, MXene nanosheets provide interconnected conductive networks, and function as “bricks” to the



**FIGURE 9** (A) Illustration showing fabrication procedure of MXene-mediated flexible wearable transient pressure sensors. Reproduced with permission.<sup>226</sup> Copyright 2019, the American Chemical Society. (B) Demonstrations of stretchability of MXene-based hydrogel (M-hydrogel); (C) photographs showing the self-healing capability of the M-hydrogel; (D–G) schematic for vocal sensing. Reproduced with permission.<sup>118</sup> Copyright 2018, the American Association for the Advancement of Science. (H) Microcontroller unit and the circuit connection settings with devices. (I) Circuit design for the signal transduction, processing, and wireless transmission. (J) Data glove mounted on the e-skin sensors for gesture recognition. (K) Gesture response at relative resistance changes of e-skins. Reproduced with permission.<sup>117</sup> Copyright 2020, the American Association for the Advancement of Science. PLA, polylactic acid

structure and other constituents, such as CNFs, act as “mortar”.<sup>36</sup> This nacre-like structure improves EMI shielding and the mechanical strength of the device. For example, Cao et al.<sup>35</sup> integrated delaminated d-Ti<sub>3</sub>C<sub>2</sub>T<sub>x</sub> MXene and CNF, mimicking the structure of the nacre. The prepared d-Ti<sub>3</sub>C<sub>2</sub>T<sub>x</sub>/CNF composite paper showed electrical conductivity up to 739.4 S m<sup>-1</sup> at a thickness of 47 μm and an excellent-specific EMI shielding efficiency up to 2647 dB cm<sup>2</sup> g<sup>-1</sup>.<sup>35</sup> Many similar structures have been reported for excellent EM wave reflection and absorption.<sup>144,166</sup>

Similarly, a bioinspired nanostructure was fabricated by layer-by-layer deposition of MXene nanosheets and AgNWs on the surface of silk textiles for EMI shielding.<sup>88</sup> The particular MXene functionalization achieved self-derived hydrophobicity, suitable for smart garments and electronic applications. Notably, the layered structure is shown to maintain two of its phases with various impedances, generating primary internal scattering at the internal interfaces, which facilitates attenuation of the incident EM radiation. Therefore, a linear improvement was achieved with different nanomaterial concentrations and overall, the composite materials demonstrated an EMI SE of ~90 dB in the spectrum of 12.4 GHz at a thickness of 450 μm.

Ti<sub>3</sub>C<sub>2</sub>T<sub>x</sub> MXene nanosheets have been assembled in several 3D architectural systems to produce materials with controllable alignment and these structures show great promise in EM wave absorption. In this sense, ultralight MXene aerogels or hydrogels have been prepared to utilize MXene in several matrix systems via various formation techniques.<sup>145</sup> Han et al.<sup>136</sup> constructed an anisotropic, additive-free, and lamellar MXene aerogel by applying a bidirectional freeze-casting approach (Figure 10A). Three different types of MXene (Ti<sub>3</sub>C<sub>2</sub>T<sub>x</sub>, Ti<sub>2</sub>CT<sub>x</sub>, and Ti<sub>3</sub>CNT<sub>x</sub>) were employed in this study and the individually-prepared aerogels exhibited an average EMI SE of 70.5, 69.2, and 54.1 dB, respectively, at a density of ≈11.0 mg cm<sup>-3</sup>. As shown in Figure 10B–D, Ti<sub>3</sub>C<sub>2</sub>T<sub>x</sub> MXene aerogel formed a lamellar structure at various densities and showed an ultrahigh specific EMI SE of 88 182 dB cm<sup>2</sup> g<sup>-1</sup> due to its low density (0.0055 g cm<sup>-3</sup>). Besides, MXene aerogel compression from 3 to 1 mm showed stability in shielding effectiveness, and high performance when compared to other devices (Figure 10E). This could be due to their formation of 3D skeletons with well-aligned cellular structure, as shown in the mechanism (Figure 10F). A similar synthetic method was applied to prepare a lamellar and porous structured aerogel by combining MXene nanosheets with 1D CNTs.<sup>147</sup> The hybrid aerogel reinforced compressive modulus by 9661% compared to the pristine MXene hydrogel, and endowed in shielding EMI waves

to a value of 103.9 dB at a thickness of 3 mm at the X-band region. MXene is also incorporated with 2D graphene to form 3D aerogel or hydrogel structures for EMI shielding, wherein graphene contributes to the 3D structural formation with strong gelation features and mechanical flexibility.<sup>146,229</sup> Zhao et al.<sup>44</sup> utilized the excellent gelation capability of graphene to manufacture a 3D porous MXene/rGO composite aerogel and the achieved cellular microstructure aerogel showed an outstanding EMI SE of 50 dB in the X-band at a low Ti<sub>3</sub>C<sub>2</sub>T<sub>x</sub> MXene content of 0.74 vol%.

Recently, Cheng and coworkers fabricated a high-performance MXene EMI shielding film through a bridging induced densification approach of hydrogen and covalent bonding (Figure 10G).<sup>228</sup> Due to the effective densification, a highly dense MXene platelet stacking was achieved, leading to superior mechanical robustness. The microstructural analysis revealed that the sequentially bridged MXene (SBM) possessed a lower porosity compared to a conventional MXene film (Figure 10H–J). The large area SBM film endowed excellent EMI shielding effectiveness even after being stored in humid air for 10 days when compared to the conventional MXene film (Figure 10K).

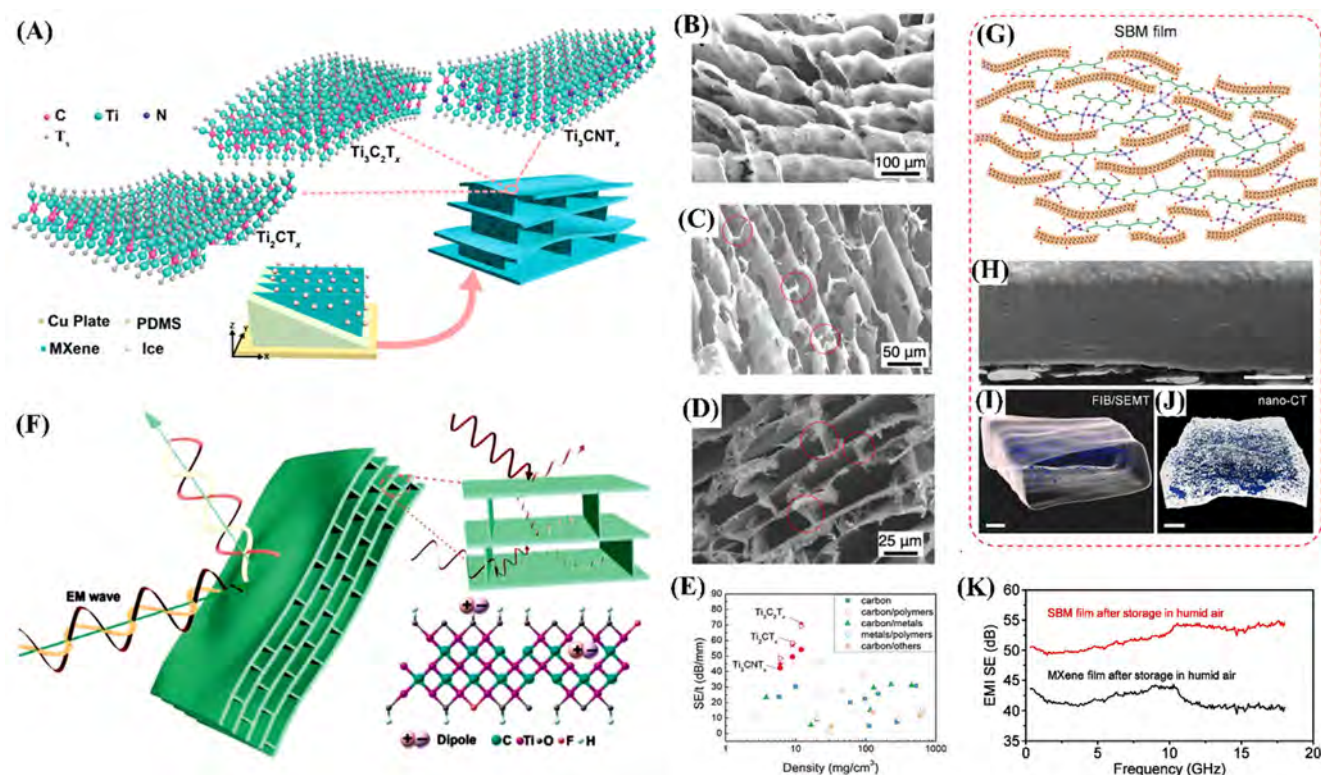
## 5 | SUMMARY AND FUTURE TRENDS

As a flourishing material of the 2D family, MXene presents enriched surface chemistry, offering tunable MXene performance for different applications, particularly in flexible electronics. As discussed in this article, MXene presents huge opportunities in designing wearable and flexible electronic devices for portable energy storage platforms, medical surveillance, HMI, and EMI shielding. The rapid development of MXene-based technologies can be observed; however, prototyping and miniaturization of electronic devices are still mainly limited to research laboratories. Eventually, newly-developed technologies are expected to complement existing electronic devices in the marketplace and create more diverse technologies with more functionality.

### 5.1 | Scalable and sustainable production of MXene

Since MXene was discovered, several strategies have been investigated to synthesize MXenes. However, technical difficulties and safety are crucial concerns in the synthesis of MXene because it involves hazardous HF solution in the reaction system. Researchers have developed





**FIGURE 10** (A) Schematic representation showing a bidirectional freeze-casting mechanism and the aligned lamellar structure with interconnected bridges of MXene aerogels obtained from various kinds of MXene flakes. (B–D) SEM images of  $Ti_3C_2T_x$  aerogels with various densities of 5.5, 8.3, and 11.0  $mg\ cm^{-3}$ , respectively. Red circle showing interlayer synapses and bridges. (E) Comparison of MXene aerogel EMI shielding performance with other reported devices. (F) Mechanism illustrating multiple reflections between the lamellae and polarizations losses from MXene flakes. Reproduced with permission.<sup>136</sup> Copyright 2019, WILEY-VCH Verlag. (G) structural model of SBM film; (H) cross-sectional SEM image of SBM film; (I, J) 3D-reconstructed void microstructures of SBM; and (K) EMI SE for MXene and SBM films in humid air conditions. Reproduced with permission.<sup>228</sup> Copyright 2021, the American Association for the Advancement of Science. EMI, electromagnetic interference; SBM, sequentially bridged MXene; SEM, scanning electron microscopy

several methods to decrease the concentration of HF, for example, a mixture of low content (5 wt%) HF and HCl were utilized to etch MAX phases, and the product quality of MXene was equivalent to that of MXene produced from highly-concentrated HF solution.<sup>230</sup> Although several salt-based etching systems have been developed to produce MXenes, a mixture of lithium fluoride and hydrochloric acid was an effective etchant for  $Ti_3AlC_2$ .<sup>231</sup> Recently, delaminated  $Ti_3C_2T_x$  MXene nanosheets were produced in batches of (1–50) grams. Importantly, wet chemical etching of MXene may increase the production scalability to more than kilograms or even quantities with tons, which can be achieved by scaling up the volume of the reactor and etchants. Besides, the quality of MXene and functional characteristics such as interlayer spacing, flake size, specific surface layer, etc. should be ensured for the device fabrication. Moreover, as it is a large family of 2D materials, exploring other types of MXene requires more rigorous efforts, promoting various features for device applications. Hence, developing

precise synthesis protocols and using advanced characterization tools to reveal the properties of MXene is also crucial.

One of the key challenges that is often encountered during the processing of MXene based devices is oxidation. MXene nanosheets tend to oxidize in the atmosphere, which is detrimental to applications involving ambient environments and long-term operation.<sup>232</sup> Apart from the synthesis parameters and quality of parent MXene, there are several factors that directly influence MXenes oxidative degradation, including storage environment, temperature, and dispersion concentration. Therefore, several investigations have been conducted to improve the oxidation stability, for example, synthesizing minimal defective layered MXenes, improving storage conditions, passivating the defects of MXene nanosheets in aqueous dispersions, replacing the water medium with organic solvents, and so forth.<sup>233</sup> Moreover, on encapsulation of MXene within a polymer matrix (e.g., PVA, polydopamine [PDA], etc.), their oxidation can be



significantly slowed down.<sup>233</sup> To date, numerous strategies have been developed to overcome the oxidative behavior of MXenes, which shows its potential in future advanced applications.

## 5.2 | Design concerns for MXene-integrated wearable electronic platforms

### 5.2.1 | Designing human-skin adaptable electronics

Skin-attachable wearable electronic devices should have sufficient adaptability and flexibility. Recently, MXene-based electrodes have been utilized for multimodal skin biosensing (ECG, EMG, and electroencephalogram [EEG] monitoring) and the devices have shown skin-adhered performance on several bending phenomena.<sup>179,234,235</sup> Owing to the excellent mechanical robustness of MXene, it has been exploited in several skin-conformal platforms. However, these devices should not pose any negative effect to human skin over long-term usage. While previous studies showed that MXene has low toxicity, more systematic studies are required to ensure its biocompatibility for bioelectronics.

### 5.2.2 | Reliability in data acquisition for mobile devices

MXene-based devices have been utilized in wearable electronics, healthcare, wireless, and HMI. For example, MXene-based electronics are now used in multiple wireless bioelectrical signal acquisition systems (ECG and EMG).<sup>235</sup> However, these biophysical data must be reliable, repeatable, and precise and any alteration in the acquisition of reliable data may seem counter-intuitive. Thus, electrodes fabricated from MXene should have high functionality, and generated signals should be free from additional noise or disturbances. However, a multidisciplinary approach is required for biophysical data analysis and signal processing to ensure the reliability and useability of the data.

### 5.2.3 | Designing functional structures with new attributes

MXene is highly compatible with other substrates or nanomaterials and therefore generates synergies in combination with others describing the effectiveness of MXene in device formation. MXene has been explored in many nanostructural formations such as 3D, 2D + 2D, 2D + 1D,

2D + 0D heterostructures for multifunctional applications. Development of several application-wise specific structures may provide high efficiency and functionality. As such, MXene-derived foam-like porous and segregated structural aerogel could be beneficial for EMI shielding applications. Likewise, several novel bioinspired structures could be a new addition for enhanced functional applications. Textile-based devices can open up more possibilities in terms of skin applications compared to other rigid and bulky structures. Overall, emphasis should be placed on developing new nanostructures with exceptional properties. This can be achievable from the rational and deliberate designation of MXene hybrid nanostructures.

### 5.2.4 | Designing all-in-one wearable solutions

While many current wearable electronic devices perform a specific function, an integrated electronic system could be promising to maximize their performances. It may be worth developing sensors that integrate more functions into a single portable platform, eliminating the need for multiple sensors or electronic modules in a body. For example, a smart-clothing system with integrated sensors for energy storage and harvesting, strain sensing, Joule heating, etc., could be promising for versatile operation with all-in-one wearable operation, compared to a single electrode. Recently, several integrated MXene electrodes have been fabricated, but they are limited to only Joule heating and strain sensing. Therefore, it is urgent to develop more integrated systems for an all-in-one wearable solution and self-powered system.

## ACKNOWLEDGMENT

The authors thank Dr. Andrew T. Smith for his assistance in drafting this article.

## CONFLICT OF INTEREST

The authors declare no conflict of interest.

## ORCID

Bapan Adak  <https://orcid.org/0000-0001-7197-082X>

Luyi Sun  <https://orcid.org/0000-0002-5419-1063>

## REFERENCES

1. Jin H, Abu-Raya YS, Haick H. Advanced materials for health monitoring with skin-based wearable devices. *Adv Healthcare Mater.* 2017;6(11):1700024.
2. Rana SMS, Rahman MT, Salaududdin M, et al. Electrospun PVDF-TrFE/MXene nanofiber mat-based triboelectric nanogenerator for smart home appliances. *ACS Appl Materials Interfaces.* 2021;13(4):4955-4967.

3. Fan FR, Tang W, Wang ZL. Flexible nanogenerators for energy harvesting and self-powered electronics. *Adv Mater*. 2016;28(22):4283-4305.
4. Shi X, Zuo Y, Zhai P, et al. Large-area display textiles integrated with functional systems. *Nature*. 2021;591(7849):240-245.
5. Wu Y, Mechael SS, Lerma C, Carmichael RS, Carmichael TB. Stretchable ultrasheer fabrics as semitransparent electrodes for wearable light-emitting e-textiles with changeable display patterns. *Matter*. 2020;2(4):882-895.
6. Sharma S, Chhetry A, Zhang S, et al. Hydrogen-bond-triggered hybrid nanofibrous membrane-based wearable pressure sensor with ultrahigh sensitivity over a broad pressure range. *ACS Nano*. 2021;15(3):4380-4393.
7. Cianchetti M, Laschi C, Menciassi A, Dario P. Biomedical applications of soft robotics. *Nature Reviews Materials*. 2018;3(6):143-153.
8. Yin R, Wang D, Zhao S, Lou Z, Shen G. Wearable sensors-enabled human-machine interaction systems: from design to application. *Adv Funct Mater*. 2021;31(11):2008936.
9. Wang C, Xia K, Wang H, Liang X, Yin Z, Zhang Y. Advanced carbon for flexible and wearable electronics. *Adv Mater*. 2019;31(9):1-37.
10. Khan Y, Ostfeld AE, Lochner CM, Pierre A, Arias AC. Monitoring of vital signs with flexible and wearable medical devices. *Adv Mater*. 2016;28(22):4373-4395.
11. Ahmed A, Jalil MA, Hossain MM, et al. A PEDOT:PSS and graphene-clad smart textile-based wearable electronic joule heater with high thermal stability. *J Mater Chem C*. 2020;8(45):16204-16215.
12. Li S, Zhang Y, Wang Y, et al. Physical sensors for skin-inspired electronics. *InfoMat*. 2020;2(1):184-211.
13. Li J, Xin M, Ma Z, Shi Y, Pan L. Nanomaterials and their applications on bio-inspired wearable electronics. *Nanotechnology*. 2021;32(47):472002.
14. Hu W, Zhang H, Salaita K, Sirringhaus H. SmartMat: smart materials to smart world. *SmartMat*. 2020;1(1):e1014.
15. Ahmed A, Hossain MM, Adak B, Mukhopadhyay S. Recent advances in 2D MXene integrated smart-textile interfaces for multifunctional applications. *Chem Mater*. 2020;32(24):10296-10320.
16. Lei JC, Zhang X, Zhou Z. Recent advances in MXene: preparation, properties, and applications. *Front Phys*. 2015;10(3):276-286.
17. VahidMohammadi A, Rosen J, Gogotsi Y. The world of two-dimensional carbides and nitrides (MXenes). *Science*. 2021;372(6547).
18. Naguib M, Kurtoglu M, Presser V, et al. Two-dimensional nanocrystals produced by exfoliation of  $\text{Ti}_3\text{AlC}_2$ . *Adv Mater*. 2011;23(37):4248-4253.
19. Gogotsi Y, Huang Q. MXenes: two-dimensional building blocks for future materials and devices. *ACS Nano*. 2021;15(4):5775-5780.
20. Anasori B, Lukatskaya MR, Gogotsi Y. 2D metal carbides and nitrides (MXenes) for energy storage. *Nat Rev Mat*. 2017;2(2):1-17.
21. Wan S, Li X, Wang Y, et al. Strong sequentially bridged MXene sheets. *Proc Natl Acad Sci U S A*. 2020;117(44):27154-27161.
22. Zhou T, Wu C, Wang Y, et al. Super-tough MXene-functionalized graphene sheets. *Nat Commun*. 2020;11(1):1-11.
23. Abdolhosseinzadeh S, Jiang X, Zhang H, Qiu J, Zhang CJ. Perspectives on solution processing of two-dimensional MXenes. *Mater Today*. 2021;48:214-240.
24. Sreenilayam SP, Ul Ahad I, Nicolosi V, Brabazon D. Mxene materials based printed flexible devices for healthcare, biomedical and energy storage applications. *Mater Today*. 2021;43:99-131.
25. Zhao L, Wang K, Wei W, Wang L, Han W. High-performance flexible sensing devices based on polyaniline/MXene nanocomposites. *InfoMat*. 2019;1(3):407-416.
26. Kim H, Alshareef HN. MXetronics: MXene-enabled electronic and photonic devices. *ACS Mater Letters*. 2020;2(1):55-70.
27. Qin R, Shan G, Hu M, Huang W. Two-dimensional transition metal carbides and/or nitrides (MXenes) and their applications in sensors. *Materials Today Phys*. 2021;21:100527.
28. Zhang C(J), Cui L, Abdolhosseinzadeh S, Heier J. Two-dimensional MXenes for lithium-sulfur batteries. *InfoMat*. 2020;2(4):613-638.
29. Choi W, Choudhary N, Han GH, Park J, Akinwande D, Lee YH. Recent development of two-dimensional transition metal dichalcogenides and their applications. *Mater Today*. 2017;20(3):116-130.
30. Faruk MO, Ahmed A, Adak B, Marzana M, Hossain MM, Mukhopadhyay S. High performance 2D MXene based conducting polymer hybrids: synthesis to emerging applications. *J Mater Chem C*. 2021;9(32):10193-10215.
31. Li K, Liang M, Wang H, et al. 3D MXene architectures for efficient energy storage and conversion. *Adv Funct Mater*. 2020;30(47):1-22.
32. Pang J, Mendes RG, Bachmatiuk A, et al. Applications of 2D MXenes in energy conversion and storage systems. *Chem Soc Rev*. 2019;48(1):72-133.
33. Xiong D, Shi Y, Yang HY. Rational design of MXene-based films for energy storage: Progress, prospects. *Mater Today*. 2021;46:183-211.
34. Luo J, Matios E, Wang H, Tao X, Li W. Interfacial structure design of MXene-based nanomaterials for electrochemical energy storage and conversion. *InfoMat*. 2020;2(6):1057-1076.
35. Cao WT, Chen FF, Zhu YJ, et al. Binary strengthening and toughening of MXene/cellulose nanofiber composite paper with nacre-inspired structure and superior electromagnetic interference shielding properties. *ACS Nano*. 2018;12(5):4583-4593.
36. Liu Z, Wang W, Tan J, et al. Bioinspired ultra-thin polyurethane/MXene nacre-like nanocomposite films with synergistic mechanical properties for electromagnetic interference shielding. *J Mater Chem C*. 2020;8(21):7170-7180.
37. Liu X, Jin X, Li L, et al. Air-permeable, multifunctional, dual-energy-driven MXene-decorated polymeric textile-based wearable heaters with exceptional electrothermal and photothermal conversion performance. *J Mater Chem A*. 2020;8(25):12526-12537.
38. Seyedin S, Uzun S, Levitt A, et al. MXene composite and coaxial fibers with high stretchability and conductivity for wearable strain sensing textiles. *Adv Funct Mater*. 2020;30(12):1910504.
39. Hasan MM, Hossain MM, Chowdhury HK. Two-dimensional MXene-based flexible nanostructures for functional nanodevices: a review. *J Mater Chem A*. 2021;9(6):3231-3269.
40. Wen D, Wang X, Liu L, et al. Inkjet printing transparent and conductive MXene ( $\text{Ti}_3\text{C}_2\text{T}_x$ ) films: a strategy for flexible

- energy storage devices. *ACS Appl Mater Interfaces*. 2021; 13(15):17766-17780.
41. Huang W, Hu L, Tang Y, Xie Z, Zhang H. Recent advances in functional 2D MXene-based nanostructures for next-generation devices. *Adv Funct Mater*. 2020;30(49):1-32.
  42. Song F, Li G, Zhu Y, Wu Z, Xie X, Zhang N. Rising from the horizon: three-dimensional functional architectures assembled with MXene nanosheets. *J Mater Chem A*. 2020;8(36):18538-18559.
  43. Gao L, Li C, Huang W, et al. MXene/polymer membranes: synthesis, properties, and emerging applications. *Chem Mater*. 2020;32(5):1703-1747.
  44. Zhao S, Bin ZH, Luo JQ, et al. Highly electrically conductive three-dimensional  $\text{Ti}_3\text{C}_2\text{T}_x$  MXene/reduced graphene oxide hybrid aerogels with excellent electromagnetic interference shielding performances. *ACS Nano*. 2018;12(11):11193-11202.
  45. Cheng Y, Ma Y, Li L, et al. Bioinspired microspines for a high-performance spray  $\text{Ti}_3\text{C}_2\text{T}_x$  MXene-based piezoresistive sensor. *ACS Nano*. 2020;14(2):2145-2155.
  46. Lipatov A, Lu H, Alhabeb M, et al. Elastic properties of 2D  $\text{Ti}_3\text{C}_2\text{T}_x$  MXene monolayers and bilayers. *Sci Adv*. 2018;4(6):eaat0491.
  47. Kurtoglu M, Naguib M, Gogotsi Y, Barsoum MW. First principles study of two-dimensional early transition metal carbides. *MRS Commun*. 2012;2(4):133-137.
  48. Lipatov A, Alhabeb M, Lu H, et al. Electrical and elastic properties of individual single-layer  $\text{Nb}_4\text{C}_3\text{T}_x$  MXene flakes. *Adv Electron Mater*. 2020;6(4):1901382.
  49. Borysiuk VN, Mochalin VN, Gogotsi Y. Molecular dynamic study of the mechanical properties of two-dimensional titanium carbides  $\text{Ti}_n\text{C}_m$  (MXenes). *Nanotechnology*. 2015; 26(26):1-10.
  50. Ibrahim Y, Mohamed A, Abdelgawad AM, Eid K, Abdullah AM, Elzatahry A. The recent advances in the mechanical properties of self-standing two-dimensional MXene-based nanostructures: deep insights into the super-capacitor. *Nanomaterials*. 2020;10(10):1-27.
  51. Zhang CJ, Anasori B, Seral-Ascaso A, et al. Transparent, flexible, and conductive 2D titanium carbide (MXene) films with high volumetric capacitance. *Adv Mater*. 2017;29(36).
  52. Levitt A, Zhang J, Dion G, Gogotsi Y, Razal JM. MXene-based fibers, yarns, and fabrics for wearable energy storage devices. *Adv Funct Mater*. 2020;30(47):1-22.
  53. Lipatov A, Alhabeb M, Lukatskaya MR, Boson A, Gogotsi Y, Sinitskii A. Effect of synthesis on quality, electronic properties and environmental stability of individual monolayer  $\text{Ti}_3\text{C}_2$  MXene flakes. *Adv Electron Mater*. 2016;2(12):1600255.
  54. Dillon AD, Ghidui MJ, Krick AL, et al. Highly conductive optical quality solution-processed films of 2D titanium carbide. *Adv Funct Mater*. 2016;26(23):4162-4168.
  55. Ahmed A, Bain S, Prottoy ZH, et al. Silk-templated nanomaterial interfaces for wearables and bioelectronics: advances and prospects. *ACS Mater Lett*. 2021;4(1):68-86.
  56. Cao C, Lin Z, Liu X, et al. Strong reduced graphene oxide coated Bombyx mori silk. *Adv Funct Mater*. 2021;31(34):2102923.
  57. Qin S, Usman KAS, Hegh D, et al. Development and applications of MXene-based functional fibers. *ACS Appl Mater Interfaces*. 2021;13(31):36655-36669.
  58. Cheng B, Wu P. Scalable fabrication of Kevlar/ $\text{Ti}_3\text{C}_2\text{T}_x$  MXene intelligent wearable fabrics with multiple sensory capabilities. *ACS Nano*. 2021;15(5):8676-8685.
  59. Hossain MM, Bradford P. Industrially knittable CNT/cotton sheath-core yarns for smart textiles. In: Kim J, ed. *Nano-, Bio-, Info-Tech Sensors, and 3D Systems IV*. Vol 11378. SPIE; 2020:9.
  60. Chatterjee K, Ghosh TK. 3D printing of textiles: potential roadmap to printing with fibers. *Adv Mater*. 2020;32(4):1902086.
  61. Hossain MM, Bradford PD. Durability of smart electronic textiles. *Nanosensors and Nanodevices for Smart Multifunctional Textiles*. Elsevier; 2021:27-53.
  62. Joshi M, Adak B. Advances in nanotechnology based functional, smart and intelligent textiles: a review. *Comprehensive Nanoscience and Nanotechnology*. Vol 1-5. Elsevier; 2019: 253-290.
  63. He J, Lu C, Jiang H, et al. Scalable production of high-performing woven lithium-ion fibre batteries. *Nature*. 2021; 597(7874):57-63.
  64. Chen G, Li Y, Bick M, Chen J. Smart textiles for electricity generation. *Chem Rev*. 2020;120(8):3668-3720.
  65. Liman MLR, Islam MT, Hossain MM. Mapping the Progress in flexible electrodes for wearable electronic textiles: materials, durability, and applications. *Adv Electron Mater*. 2021; 8(1):2100578.
  66. Eskandarian L, Lam E, Rupnow C, Meghbrazi MA, Naguib HE. Robust and multifunctional conductive yarns for biomedical textile computing. *ACS Appl Electron Mater*. 2020; 2(6):1554-1566.
  67. Karim N, Afroj S, Lloyd K, et al. Sustainable personal protective clothing for healthcare applications: a review. *ACS Nano*. 2020;14(10):12313-12340.
  68. Yapici MK, Alkhdhir TE. Intelligent medical garments with graphene-functionalized smart-cloth ECG sensors. *Sensors (Switzerland)*. 2017;17(4):1-12.
  69. Shi J, Liu S, Zhang L, et al. Smart textile-integrated microelectronic systems for wearable applications. *Adv Mater*. 2020; 32(5):1901958.
  70. Wang X, Liu Z, Zhang T. Flexible sensing electronics for wearable/attachable health monitoring. *Small*. 2017;13(25): 1602790.
  71. Atalay A, Sanchez V, Atalay O, et al. Batch fabrication of customizable silicone-textile composite capacitive strain sensors for human motion tracking. *Adv Mater Technol*. 2017;2(9):1700136.
  72. Zhao J, Fu Y, Xiao Y, Dong Y, Wang X, Lin L. A naturally integrated smart textile for wearable electronics applications. *Adv Mater Technol*. 2020;5(1):1900781.
  73. Abdullah al Rumon M, Shahriar H. Fabrication of interdigitated capacitor on fabric as tactile sensor. *Sensors Int*. 2021;2: 100086.
  74. Shi M, Shen M, Guo X, et al.  $\text{Ti}_3\text{C}_2\text{T}_x$ MXene-decorated nanoporous polyethylene textile for passive and active personal precision heating. *ACS Nano*. 2021;15(7):11396-11405.
  75. Faruk MO, Ahmed A, Jalil MA, et al. Functional textiles and composite based wearable thermal devices for joule heating: progress and perspectives. *Appl Mater Today*. 2021; 23:101025.
  76. Bhattacharjee S, Joshi R, Chughtai AA, Macintyre CR. Graphene modified multifunctional personal protective clothing. *Adv Mater Interfaces*. 2019;6(21):1900622.



77. Tabor J, Chatterjee K, Ghosh TK. Smart textile-based personal thermal comfort systems: current status and potential solutions. *Adv Mater Technol*. 2020;5(5):1901155.
78. Zhao X, Wang LY, Tang CY, et al. Smart  $\text{Ti}_3\text{C}_2\text{T}_x$ /MXene fabric with fast humidity response and joule heating for healthcare and medical therapy applications. *ACS Nano*. 2020;14(7):8793-8805.
79. Sanchez V, Walsh CJ, Wood RJ. Textile technology for soft robotic and autonomous garments. *Adv Funct Mater*. 2021;31(6):2008278.
80. Ruckdashel RR, Venkataraman D, Park JH. Smart textiles: a toolkit to fashion the future. *J Appl Phys*. 2021;129(13):130903.
81. Levitt A, Hegh D, Phillips P, et al. 3D knitted energy storage textiles using MXene-coated yarns. *Mater Today*. 2020;34:17-29.
82. Levitt A, Seyedin S, Zhang J, et al. Bath electrospinning of continuous and scalable multifunctional MXene-infiltrated nanoyarns. *Small*. 2020;16(26):2002158.
83. Zhang J, Uzun S, Seyedin S, et al. Additive-free MXene liquid crystals and fibers. *ACS Central Sci*. 2020;6(2):254-265.
84. Shin H, Eom W, Lee KH, Jeong W, Kang DJ, Han TH. Highly electroconductive and mechanically strong  $\text{Ti}_3\text{C}_2\text{T}_x$ /MXene fibers using a deformable MXene gel. *ACS Nano*. 2021;15(2):3320-3329.
85. Zhang X, Wang X, Lei Z, et al. Flexible MXene-decorated fabric with interwoven conductive networks for integrated joule heating, electromagnetic interference shielding, and strain sensing performances. *ACS Appl Mater Interfaces*. 2020;12(12):14459-14467.
86. Jiang Q, Kurra N, Alhabeb M, Gogotsi Y, Alshareef HN. All pseudocapacitive MXene- $\text{RuO}_2$  asymmetric supercapacitors. *Adv Energy Mater*. 2018;8(13):1-10.
87. Levitt AS, Alhabeb M, Hatter CB, Sarycheva A, Dion G, Gogotsi Y. Electrospun MXene/carbon nanofibers as supercapacitor electrodes. *J Mater Chem A*. 2019;7(1):269-277.
88. Liu LX, Chen W, HB Z, Wang QW, Guan F, Yu ZZ. Flexible and multifunctional silk textiles with biomimetic leaf-like MXene/silver nanowire nanostructures for electromagnetic interference shielding, humidity monitoring, and self-derived hydrophobicity. *Adv Funct Mater*. 2019;29(44):1-10.
89. Cheng W, Zhang Y, Tian W, et al. Highly efficient MXene-coated flame retardant cotton fabric for electromagnetic interference shielding. *Ind Eng Chem Res*. 2020;59(31):14025-14036.
90. Wang QW, Bin ZH, Liu J, et al. Multifunctional and water-resistant MXene-decorated polyester textiles with outstanding electromagnetic interference shielding and joule heating performances. *Adv Funct Mater*. 2019;29(7):1-10.
91. Liu R, Li J, Li M, et al. MXene-coated air-permeable pressure-sensing fabric for smart wear. *ACS Appl Mater Interfaces*. 2020;12(41):46446-46454.
92. Li T, Chen L, Yang X, et al. A flexible pressure sensor based on an MXene-textile network structure. *J Mater Chem C*. 2019;7(4):1022-1027.
93. Pu JH, Zhao X, Zha XJ, et al. Multilayer structured AgNW/WPU-MXene fiber strain sensors with ultrahigh sensitivity and a wide operating range for wearable monitoring and healthcare. *J Mater Chem A*. 2019;7(26):15913-15923.
94. Yuan L, Zhang M, Zhao T, et al. Flexible and breathable strain sensor with high performance based on MXene/nylon fabric network. *Sensors Actuators A Phys*. 2020;315:112192.
95. Li Q, Yin R, Zhang D, et al. Flexible conductive MXene/cellulose nanocrystal coated nonwoven fabrics for tunable wearable strain/pressure sensors. *J Mater Chem A*. 2020;8(40):21131-21141.
96. Wang S, Du X, Luo Y, et al. Hierarchical design of waterproof, highly sensitive, and wearable sensing electronics based on MXene-reinforced durable cotton fabrics. *Chem Eng J*. 2021;408:127363.
97. Luo J, Gao S, Luo H, et al. Superhydrophobic and breathable smart MXene-based textile for multifunctional wearable sensing electronics. *Chem Eng J*. 2021;406:126898.
98. Li X, Hao J, Liu R, et al. Interfacing MXene flakes on fiber fabric as an ultrafast electron transport layer for high performance textile electrodes. *Energy Storage Mater*. 2020;33:62-70.
99. Seyedin S, Yanza ERS, Razal JM. Knittable energy storing fiber with high volumetric performance made from predominantly MXene nanosheets. *J Mater Chem A*. 2017;5(46):24076-24082.
100. Zhang J, Seyedin S, Qin S, et al. Highly conductive  $\text{Ti}_3\text{C}_2\text{T}_x$ /MXene hybrid fibers for flexible and elastic fiber-shaped supercapacitors. *Small*. 2019;15(8):1804732.
101. Yan J, Ma Y, Zhang C, et al. Polypyrrole-MXene coated textile-based flexible energy storage device. *RSC Adv*. 2018;8(69):39742-39748.
102. Uzun S, Seyedin S, Stoltzfus AL, et al. Knittable and washable multifunctional MXene-coated cellulose yarns. *Adv Funct Mater*. 2019;29(45):1-13.
103. Shao W, Tebyetekerwa M, Marriam I, et al. Polyester@MXene nanofibers-based yarn electrodes. *J Power Sources*. 2018;396:683-690.
104. Park TH, Yu S, Koo M, et al. Shape-adaptable 2D titanium carbide (MXene) heater. *ACS Nano*. 2019;13(6):6835-6844.
105. Zheng X, Shen J, Hu Q, et al. Vapor phase polymerized conducting polymer/MXene textiles for wearable electronics. *Nanoscale*. 2021;13(3):1832-1841.
106. Ma C, Yuan Q, Du H, Ma MG, Si C, Wan P. Multiresponsive MXene ( $\text{Ti}_3\text{C}_2\text{T}_x$ )-decorated textiles for wearable thermal management and human motion monitoring. *ACS Appl Mater Interfaces*. 2020;12(30):34226-34234.
107. Uzun S, Han M, Strobel CJ, et al. Highly conductive and scalable  $\text{Ti}_3\text{C}_2\text{T}_x$ -coated fabrics for efficient electromagnetic interference shielding. *Carbon*. 2021;174:382-389.
108. Cao W, Ma C, Tan S, Ma M, Wan P, Chen F. Ultrathin and flexible CNTs/MXene/cellulose nanofibrils composite paper for electromagnetic interference shielding. *Nano-Micro Letters*. 2019;11(1):1-17.
109. Raagulan K, Braveenth R, Jang HJ, et al. Fabrication of non-wetting flexible free-standing MXene-carbon fabric for electromagnetic shielding in S-band region. *Bulletin Korean Chem Soc*. 2018;39(12):1412-1419.
110. Xie F, Jia F, Zhuo L, et al. Ultrathin MXene/aramid nanofiber composite paper with excellent mechanical properties for efficient electromagnetic interference shielding. *Nanoscale*. 2019;11(48):23382-23391.
111. Jia X, Shen B, Zhang L, Zheng W. Waterproof MXene-decorated wood-pulp fabrics for high-efficiency electromagnetic interference shielding and joule heating. *Compos Part B Eng*. 2020;198:108250.
112. Zhang YZ, El-Demellawi JK, Jiang Q, et al. MXene hydrogels: fundamentals and applications. *Chem Soc Rev*. 2020;49(20):7229-7251.

113. Fu F, Wang J, Zeng H, Yu J. Functional conductive hydrogels for bioelectronics. *ACS Mater Letters*. 2020;2(10):1287-1301.
114. Chen H, Ma H, Zhang P, Wen Y, Qu L, Li C. Pristine titanium carbide MXene hydrogel matrix. *ACS Nano*. 2020;14(8):10471-10479.
115. Wang Q, Pan X, Wang X, et al. Fabrication strategies and application fields of novel 2D  $\text{Ti}_3\text{C}_2\text{T}_x$  (MXene) composite hydrogels: a mini-review. *Ceram Int*. 2021;47(4):4398-4403.
116. Wang Q, Pan X, Lin C, et al. Modified  $\text{Ti}_3\text{C}_2\text{T}_x$  (MXene) nanosheet-catalyzed self-assembled, anti-aggregated, ultra-stretchable, conductive hydrogels for wearable bioelectronics. *Chem Eng J*. 2020;401:126129.
117. Cai Y, Shen J, Yang CW, et al. Mixed-dimensional MXene-hydrogel heterostructures for electronic skin sensors with ultrabroad working range. *Sci Adv*. 2020;6(48):eabb5367.
118. Zhang YZ, Lee KH, Anjum DH, et al. MXenes stretch hydrogel sensor performance to new limits. *Sci Adv*. 2018;4(6):1-8.
119. Lin Z, Barbara D, Taberna PL, et al. Capacitance of  $\text{Ti}_3\text{C}_2\text{T}_x$  MXene in ionic liquid electrolyte. *J Power Sources*. 2016;326:575-579.
120. Zhang H, Zhang P, Zheng W, et al. 3D d- $\text{Ti}_3\text{C}_2$  xerogel framework decorated with core-shell  $\text{SnO}_2@\text{C}$  for high-performance lithium-ion batteries. *Electrochim Acta*. 2018;285:94-102.
121. Liao H, Guo X, Wan P, Yu G. Conductive MXene nanocomposite organohydrogel for flexible, healable, low-temperature tolerant strain sensors. *Adv Funct Mater*. 2019;29(39):1-9.
122. Zhang J, Wan L, Gao Y, et al. Highly stretchable and self-healable MXene/polyvinyl alcohol hydrogel electrode for wearable capacitive electronic skin. *Adv Electron Mater*. 2019;5(7):1-10.
123. Wang Q, Pan X, Wang X, et al. Spider web-inspired ultra-stable 3D  $\text{Ti}_3\text{C}_2\text{T}_x$  (MXene) hydrogels constructed by temporary ultrasonic alignment and permanent in-situ self-assembly fixation. *Compos Part B Eng*. 2020;197:108187.
124. Ge G, Zhang YZ, Zhang W, et al.  $\text{Ti}_3\text{C}_2\text{T}_x$ MXene-activated fast gelation of stretchable and self-healing hydrogels: a molecular approach. *ACS Nano*. 2021;15(2):2698-2706.
125. Zhang Y, Chen K, Li Y, et al. High-strength, self-healable, temperature-sensitive, MXene-containing composite hydrogel as a smart compression sensor. *ACS Appl Mater Interfaces*. 2019;11(50):47350-47357.
126. Zhou H, Wang Z, Zhao W, et al. Robust and sensitive pressure/strain sensors from solution processable composite hydrogels enhanced by hollow-structured conducting polymers. *Chem Eng J*. 2021;403:126307.
127. Shang T, Lin Z, Qi C, et al. 3D macroscopic architectures from self-assembled MXene hydrogels. *Adv Funct Mater*. 2019;29(33):1-8.
128. Zhang L, Or SW. Self-assembled three-dimensional macroscopic graphene/MXene-based hydrogel as electrode for supercapacitor. *APL Mater*. 2020;8(9):091101.
129. Rafieerad A, Sequiera GL, Yan W, Kaur P, Amiri A, Dhingra S. Sweet-MXene hydrogel with mixed-dimensional components for biomedical applications. *J Mech Behav Biomed Mater*. 2020;101:103440.
130. Xing C, Chen S, Liang X, et al. Two-dimensional MXene ( $\text{Ti}_3\text{C}_2$ )-integrated cellulose hydrogels: toward smart three-dimensional network Nanoplatfoms exhibiting light-induced swelling and bimodal Photothermal/chemotherapy anticancer activity. *ACS Appl Mater Interfaces*. 2018;10(33):27631-27643.
131. Lukatskaya MR, Kota S, Lin Z, et al. Ultra-high-rate pseudocapacitive energy storage in two-dimensional transition metal carbides. *Nat Energy*. 2017;6(8):1-12.
132. Kayali E, Vahidmohammadi A, Orangi J, Beidaghi M. Controlling the dimensions of 2D MXenes for ultrahigh-rate pseudocapacitive energy storage. *ACS Appl Mater Interfaces*. 2018;10(31):25949-25954.
133. Deng Y, Shang T, Wu Z, et al. Fast gelation of  $\text{Ti}_3\text{C}_2\text{T}_x$  MXene initiated by metal ions. *Adv Mater*. 2019;31(43):1902432.
134. Shi S, Qian B, Wu X, et al. Self-assembly of MXene-surfactants at liquid-liquid interfaces: from structured liquids to 3D aerogels. *Angewandte Chemie - Int Ed*. 2019;58(50):18171-18176.
135. Bian R, He G, Zhi W, Xiang S, Wang T, Cai D. Ultralight MXene-based aerogels with high electromagnetic interference shielding performance. *J Mater Chem C*. 2019;7(3):474-478.
136. Han M, Yin X, Hantanasirisakul K, et al. Anisotropic MXene aerogels with a mechanically tunable ratio of electromagnetic wave reflection to absorption. *Adv Opt Mater*. 2019;7(10):1900267.
137. Zhu M, Yue Y, Cheng Y, et al. Hollow MXene sphere/reduced graphene aerogel composites for piezoresistive sensor with ultra-high sensitivity. *Adv Electron Mater*. 2020;6(2):1-9.
138. Bi L, Yang Z, Chen L, Wu Z, Ye C. Compressible AgNWs/ $\text{Ti}_3\text{C}_2\text{T}_x$ MXene aerogel-based highly sensitive piezoresistive pressure sensor as versatile electronic skins. *J Mater Chem A*. 2020;8(38):20030-20036.
139. Ma Y, Yue Y, Zhang H, et al. 3D Synergistical MXene/reduced graphene oxide aerogel for a piezoresistive sensor. *ACS Nano*. 2018;12(4):3209-3216.
140. Wang L, Zhang M, Yang B, Tan J, Ding X. Highly compressible, thermally stable, light-weight, and robust aramid nanofibers/ $\text{Ti}_3\text{AlC}_2$ MXene composite aerogel for sensitive pressure sensor. *ACS Nano*. 2020;14(8):10633-10647.
141. Li Y, Meng F, Mei Y, et al. Electrospun generation of  $\text{Ti}_3\text{C}_2\text{T}_x$  MXene@graphene oxide hybrid aerogel microspheres for tunable high-performance microwave absorption. *Chem Eng J*. 2020;391:123512.
142. Yang M, Yuan Y, Li Y, et al. Anisotropic electromagnetic absorption of aligned  $\text{Ti}_3\text{C}_2\text{T}_x$ MXene/gelatin nanocomposite aerogels. *ACS Appl Mater Interfaces*. 2020;12(29):33128-33138.
143. Dai Y, Wu X, Liu Z, Bin ZH, Yu ZZ. Highly sensitive, robust and anisotropic MXene aerogels for efficient broadband microwave absorption. *Compos Part B Eng*. 2020;200:108263.
144. Jiang Y, Xie X, Chen Y, Liu Y, Yang R, Sui G. Hierarchically structured cellulose aerogels with interconnected MXene networks and their enhanced microwave absorption properties. *J Mater Chem C*. 2018;6(32):8679-8687.
145. Liu J, Zhang HB, Xie X, et al. Multifunctional, Superelastic, and lightweight MXene/polyimide aerogels. *Small*. 2018;14(45):1-10.
146. Wang L, Liu H, Lv X, Cui G, Gu G. Facile synthesis 3D porous MXene  $\text{Ti}_3\text{C}_2\text{T}_x@\text{RGO}$  composite aerogel with excellent dielectric loss and electromagnetic wave absorption. *J Alloys Compd*. 2020;828:154251.
147. Sambyal P, Iqbal A, Hong J, et al. Ultralight and mechanically robust  $\text{Ti}_3\text{C}_2\text{T}_x$  hybrid aerogel reinforced by carbon nanotubes

- for electromagnetic interference shielding. *ACS Appl Mater Interfaces*. 2019;11(41):38046-38054.
148. Wang Q, Wang S, Guo X, et al. MXene-reduced graphene oxide aerogel for aqueous zinc-ion hybrid supercapacitor with Ultralong cycle life. *Adv Electron Mater*. 2019;5(12):1-8.
  149. Song J, Guo X, Zhang J, et al. Rational design of free-standing 3D porous MXene/rGO hybrid aerogels as polysulfide reservoirs for high-energy lithium-sulfur batteries. *J Mater Chem A*. 2019;7(11):6507-6513.
  150. Yue Y, Liu N, Ma Y, et al. Highly self-healable 3D micro-supercapacitor with MXene-graphene composite aerogel. *ACS Nano*. 2018;12(5):4224-4232.
  151. Zhang X, Lv R, Wang A, Guo W, Liu X, Luo J. MXene aerogel scaffolds for high-rate lithium metal anodes. *Angewandte Chemie*. 2018;130(46):15248-15253.
  152. Chen X, Jiang J, Yang G, Li C, Li Y. Bioinspired wood-like coaxial fibers based on MXene@graphene oxide with superior mechanical and electrical properties. *Nanoscale*. 2020;12(41):21325-21333.
  153. Wang D, Wang L, Lou Z, et al. Biomimetic, biocompatible and robust silk fibroin-MXene film with stable 3D cross-link structure for flexible pressure sensors. *Nano Energy*. 2020;78:105252.
  154. Zhao Q, Wang Y, Cui H, Du X. Bio-inspired sensing and actuating materials. *J Mater Chem C*. 2019;7(22):6493-6511.
  155. Peng J, Cheng Q. High-performance nanocomposites inspired by nature. *Adv Mater*. 2017;29(45):1702959.
  156. Ahmed A, Adak B, Faruk MO, Mukhopadhyay S. Nanocellulose coupled 2D graphene nanostructures: emerging paradigm for sustainable functional applications. *Ind Eng Chem Res*. 2021;60(30):10882-10916.
  157. Srivatsa S, Paćko P, Mishnaevsky L, Uhl T, Grabowski K. Deformation of bioinspired MXene-based polymer composites with brick and mortar structures: a computational analysis. *Materials*. 2020;13(22):1-19.
  158. Hou K, Nie Y, Tendo Mugaanire I, Guo Y, Zhu M. A novel leaf inspired hydrogel film based on fiber reinforcement as rapid steam sensor. *Chem Eng J*. 2020;382:122948.
  159. Zhang Y, Gong S, Zhang Q, et al. Graphene-based artificial nacre nanocomposites. *Chem Soc Rev*. 2016;45(9):2378-2395.
  160. Gong S, Ni H, Jiang L, Cheng Q. Learning from nature: constructing high performance graphene-based nanocomposites. *Mater Today*. 2017;20(4):210-219.
  161. Huang C, Peng J, Cheng Y, et al. Ultratough nacre-inspired epoxy-graphene composites with shape memory properties. *J Mater Chem A*. 2019;7(6):2787-2794.
  162. Christian M, Mazzaro R, Morandi V. Bioinspired design of graphene-based materials. *Adv Funct Mater*. 2020;30(51):1-26.
  163. Wan S, Peng J, Jiang L, Cheng Q. Bioinspired graphene-based nanocomposites and their application in flexible energy devices. *Adv Mater*. 2016;28(36):7862-7898.
  164. Wang K, Lou Z, Wang L, et al. Bioinspired interlocked structure-induced high deformability for two-dimensional titanium carbide (MXene)/natural microcapsule-based flexible pressure sensors. *ACS Nano*. 2019;13(8):9139-9147.
  165. Das P, Mai VC, Duan H. Flexible bioinspired ternary nanocomposites based on Carboxymethyl cellulose/Nanoclay/graphene oxide. *ACS Appl Polymer Mater*. 2019;1(6):1505-1513.
  166. Liang C, Qiu H, Song P, Shi X, Kong J, Gu J. Ultra-light MXene aerogel/wood-derived porous carbon composites with wall-like "mortar/brick" structures for electromagnetic interference shielding. *Sci Bull*. 2020;65(8):616-622.
  167. Wang Z, Han X, Han X, Chen Z, Wang S, Pu J. MXene/wood-derived hierarchical cellulose scaffold composite with superior electromagnetic shielding. *Carbohydr Polym*. 2021;254:117033.
  168. Shi X, Wang H, Xie X, et al. Bioinspired ultrasensitive and stretchable MXene-based strain sensor via nacre-mimetic microscale "brick-and-mortar" architecture. *ACS Nano*. 2019;13(1):649-659.
  169. Cai G, Ciou JH, Liu Y, Jiang Y, Lee PS. Leaf-inspired multi-responsive MXene-based actuator for programmable smart devices. *Sci Adv*. 2019;5(7):eaaw7956.
  170. Zhao H, Guo L. Nacre-inspired structural composites: performance-enhancement strategy and perspective. *Adv Mater*. 2017;29(45):1702903.
  171. Zhao H, Yang Z, Guo L. Nacre-inspired composites with different macroscopic dimensions: strategies for improved mechanical performance and applications. *NPG Asia Mater*. 2018;10(4):1-22.
  172. Xin W, Xi GQ, Cao WT, et al. Lightweight and flexible MXene/CNF/silver composite membranes with a brick-like structure and high-performance electromagnetic-interference shielding. *RSC Adv*. 2019;9(51):29636-29644.
  173. Zhou H, Li X, Fan T, et al. Artificial inorganic leaves for efficient photochemical hydrogen production inspired by natural photosynthesis. *Adv Mater*. 2010;22(9):951-956.
  174. Zhang YZ, Wang Y, Jiang Q, El-Demellawi JK, Kim H, Alshareef HN. MXene printing and patterned coating for device applications. *Adv Mater*. 2020;32(21):1908486.
  175. Hasan MM, Hossain MM. Nanomaterials-patterned flexible electrodes for wearable health monitoring: a review. *J Mater Sci*. 2021;56(27):14900-14942.
  176. Sajedi-Moghaddam A, Rahmanian E, Naseri N. Inkjet-printing technology for supercapacitor application: current state and perspectives. *ACS Appl Mater Interfaces*. 2020;12(31):34487-34504.
  177. Jabari E, Ahmed F, Liravi F, Secor EB, Lin L, Toyserkani E. 2D printing of graphene: a review. *2D Mater*. 2019;6(4):042004.
  178. Uzun S, Schelling M, Hantanasirisakul K, et al. Additive-free aqueous MXene inks for thermal inkjet printing on textiles. *Small*. 2021;17(1):1-12.
  179. Saleh A, Wustoni S, Bihar E, et al. Inkjet-printed  $\text{Ti}_3\text{C}_2\text{T}_x$  MXene electrodes for multimodal cutaneous biosensing. *J Phys Mater*. 2020;3(4):44004.
  180. Zhang C, McKeon L, Kremer MP, et al. Additive-free MXene inks and direct printing of micro-supercapacitors. *Nat Commun*. 2019;10(1):1-9.
  181. Vural M, Pena-Francesch A, Bars-Pomes J, et al. Inkjet printing of self-assembled 2D titanium carbide and protein electrodes for stimuli-responsive electromagnetic shielding. *Adv Funct Mater*. 2018;28(32):1-10.
  182. Wu CW, Unnikrishnan B, Chen IWP, Harroun SG, Chang HT, Huang CC. Excellent oxidation resistive MXene aqueous ink for micro-supercapacitor application. *Energy Storage Mater*. 2020;25:563-571.



183. Redondo E, Pumera M. MXene-functionalised 3D-printed electrodes for electrochemical capacitors. *Electrochem Commun.* 2021;124:106920.
184. Cao W, Ma C, Mao D, Zhang J, Ma M, Chen F. MXene-reinforced cellulose nanofibril inks for 3D-printed smart fibres and textiles. *Adv Funct Mater.* 2019;29(51):1905898.
185. Yang W, Yang J, Byun JJ, et al. 3D printing of freestanding MXene architectures for current-collector-free supercapacitors. *Adv Mater.* 2019;31(37):1-8.
186. Xu S, Dall'Agnese Y, Wei G, Zhang C, Gogotsi Y, Han W. Screen-printable microscale hybrid device based on MXene and layered double hydroxide electrodes for powering force sensors. *Nano Energy.* 2018;50:479-488.
187. Yu L, Fan Z, Shao Y, Tian Z, Sun J, Liu Z. Versatile N-doped MXene ink for printed electrochemical energy storage application. *Adv Energy Mater.* 2019;9(34):1-8.
188. Abdolhosseinzadeh S, Schneider R, Verma A, Heier J, Nüesch F, Zhang C. Turning trash into treasure: additive free MXene sediment inks for screen-printed micro-supercapacitors. *Adv Mater.* 2020;32(17):1-9.
189. Liao M, Ye L, Zhang Y, Chen T, Peng H. The recent advance in fiber-shaped energy storage devices. *Adv Electron Mater.* 2019;5(1):1800456.
190. Zhu J, Chronos A, Eppinger J, Schwingenschlögl U. S-functionalized MXenes as electrode materials for Li-ion batteries. *Appl Mater Today.* 2016;5:19-24.
191. Lin Z, Goikolea E, Balducci A, et al. Materials for supercapacitors: when Li-ion battery power is not enough. *Mater Today.* 2018;21(4):419-436.
192. Sun S, Liao C, Hafez AM, Zhu H, Wu S. Two-dimensional MXenes for energy storage. *Chem Eng J.* 2018;338:27-45.
193. Lin Z, Shao H, Xu K, Taberna PL, Simon P. MXenes as high-rate electrodes for energy storage. *Trends Chem.* 2020;2(7):654-664.
194. Han J, Wang S, Zhu S, et al. Electrospun core-shell nanofibrous membranes with nanocellulose-stabilized carbon nanotubes for use as high-performance flexible supercapacitor electrodes with enhanced water resistance, thermal stability, and mechanical toughness. *ACS Appl Mater Interfaces.* 2019;11(47):44624-44635.
195. Wang L, Fu X, He J, et al. Application challenges in fiber and textile electronics. *Adv Mater.* 2020;32(5):1-25.
196. Yang Q, Xu Z, Fang B, et al. MXene/graphene hybrid fibers for high performance flexible supercapacitors. *J Mater Chem A.* 2017;5(42):22113-22119.
197. Lee JA, Shin MK, Kim SH, et al. Ultrafast charge and discharge bistructured yarn supercapacitors for textiles and micro-devices. *Nat Commun.* 2013;4(1):1-8.
198. Wang Z, Qin S, Seyedin S, et al. High-performance bistructured MXene/carbon nanotube yarn supercapacitors. *Small.* 2018;14(37):1802225.
199. Park JW, Lee DY, Kim H, et al. Highly loaded MXene/carbon nanotube yarn electrodes for improved asymmetric supercapacitor performance. *MRS Commun.* 2019;9(1):114-121.
200. Yu C, Gong Y, Chen R, et al. A solid-state fibriform supercapacitor boosted by host-guest hybridization between the carbon nanotube scaffold and MXene nanosheets. *Small.* 2018;14(29):1-7.
201. Zhang J, Seyedin S, Gu Z, Yang W, Wang X, Razal JM. MXene: a potential candidate for yarn supercapacitors. *Nanoscale.* 2017;9(47):18604-18608.
202. Zhang W, Ma J, Zhang W, et al. A multidimensional nanostructural design towards electrochemically stable and mechanically strong hydrogel electrodes. *Nanoscale.* 2020;12(12):6637-6643.
203. Li H, Li X, Liang J, Chen Y. Hydrous RuO<sub>2</sub>-decorated MXene coordinating with silver nanowire inks enabling fully printed micro-supercapacitors with extraordinary volumetric performance. *Adv Energy Mater.* 2019;9(15):1-13.
204. Orangi J, Hamade F, Davis VA, Beidaghi M. 3D printing of additive-free 2D Ti<sub>3</sub>C<sub>2</sub>T<sub>x</sub> (MXene) ink for fabrication of micro-supercapacitors with ultra-high energy densities. *ACS Nano.* 2020;14(1):640-650.
205. He N, Patil S, Qu J, Liao J, Zhao F, Gao W. Effects of electrolyte mediation and MXene size in fiber-shaped supercapacitors. *ACS Appl Energy Mater.* 2020;3(3):2949-2958.
206. Bairagi S, Banerjee S, Chowdhury A, Ali SW. Development of a sustainable and flexible piezoelectric-cum-triboelectric energy harvester comprising a simple commodity cotton fabric. *ACS Sustain Chem Eng.* 2021;9(11):4004-4013.
207. Nam S, Kim JN, Oh S, Kim J, Ahn CW, Oh IK. Ti<sub>3</sub>C<sub>2</sub>T<sub>x</sub>MXene for wearable energy devices: supercapacitors and triboelectric nanogenerators. *APL Mater.* 2020;8(11):110701.
208. Bhatta T, Maharjan P, Cho H, et al. High-performance triboelectric nanogenerator based on MXene functionalized polyvinylidene fluoride composite nanofibers. *Nano Energy.* 2021;81:105670.
209. Salauddin M, Rana SMS, Sharifuzzaman M, et al. A novel MXene/Ecoflex nanocomposite-coated fabric as a highly negative and stable friction layer for high-output triboelectric nanogenerators. *Adv Energy Mater.* 2021;11(1):1-12.
210. Cao WT, Ouyang H, Xin W, et al. A stretchable highoutput triboelectric nanogenerator improved by MXene liquid electrode with high electronegativity. *Adv Funct Mater.* 2020;30(50):1-10.
211. Xiong J, Lin MF, Wang J, Gaw SL, Parida K, Lee PS. Wearable all-fabric-based triboelectric generator for water energy harvesting. *Adv Energy Mater.* 2017;7(21):1701243.
212. Nichols WW. Clinical measurement of arterial stiffness obtained from noninvasive pressure waveforms. *Am J Hypertens.* 2005;18(1 Pt 2):3-10.
213. Blacher J, Asmar R, Djane S, London GM, Safar ME. Aortic pulse wave velocity as a marker of cardiovascular risk in hypertensive patients. *Hypertension.* 1999;33(5):1111-1117.
214. Park Y, Shim J, Jeong S, et al. Microtopography-guided conductive patterns of liquid-driven graphene nanoplatelet networks for stretchable and skin-conformal sensor array. *Adv Mater.* 2017;29(21):1606453.
215. Yang T, Jiang X, Zhong Y, et al. A wearable and highly sensitive graphene strain sensor for precise home-based pulse wave monitoring. *ACS Sensors.* 2017;2(7):967-974.
216. Luo N, Dai W, Li C, et al. Flexible piezoresistive sensor patch enabling ultralow power cuffless blood pressure measurement. *Adv Funct Mater.* 2016;26(8):1178-1187.
217. Sharma S, Chhetry A, Sharifuzzaman M, Yoon H, Park JY. Wearable capacitive pressure sensor based on MXene composite nanofibrous scaffolds for reliable human physiological signal acquisition. *ACS Appl Mater Interfaces.* 2020;12(19):22212-22224.

218. Song D, Li X, Li XP, Jia X, Min P, Yu ZZ. Hollow-structured MXene-PDMS composites as flexible, wearable and highly bendable sensors with wide working range. *J Colloid Interface Sci.* 2019;555:751-758.
219. Darabi MA, Khosrozadeh A, Mbeleck R, et al. Skin-inspired multifunctional autonomic-intrinsic conductive self-healing hydrogels with pressure sensitivity, stretchability, and 3D printability. *Adv Mater.* 2017;29(31):1700533.
220. Lei Z, Wang Q, Sun S, Zhu W, Wu P. A bioinspired mineral hydrogel as a self-healable, mechanically adaptable ionic skin for highly sensitive pressure sensing. *Adv Mater.* 2017;29(22):1700321.
221. Lei Z, Wu P. A supramolecular biomimetic skin combining a wide spectrum of mechanical properties and multiple sensory capabilities. *Nat Commun.* 2018;9(1):1-7.
222. Boutry CM, Negre M, Jorda M, et al. A hierarchically patterned, bioinspired e-skin able to detect the direction of applied pressure for robotics. *Sci Robot.* 2018;3(24):eaau6914.
223. Park J, Lee Y, Hong J, et al. Tactile-direction-sensitive and stretchable electronic skins based on human-skin-inspired interlocked microstructures. *ACS Nano.* 2014;8(12):12020-12029.
224. Park J, Kim J, Hong J, et al. Tailoring force sensitivity and selectivity by microstructure engineering of multidirectional electronic skins. *NPG Asia Mater.* 2018;10(4):163-176.
225. Wang T, Zhang Y, Liu Q, et al. A self-healable, highly stretchable, and solution processable conductive polymer composite for ultrasensitive strain and pressure sensing. *Adv Funct Mater.* 2018;28(7):1705551.
226. Guo Y, Zhong M, Fang Z, Wan P, Yu G. A wearable transient pressure sensor made with MXene nanosheets for sensitive broad-range human-machine interfacing. *Nano Lett.* 2019;19(2):1143-1150.
227. Iqbal A, Sambyal P, Koo CM. 2D MXenes for electromagnetic shielding: a review. *Adv Funct Mater.* 2020;30(47):1-25.
228. Wan S, Li X, Chen Y, et al. High-strength scalable MXene sheets via bridging-induced densification. *Science.* 2021;374(6563):96-99.
229. Raagulan K, Kim BM, Chai KY. Recent advancement of electromagnetic interference (EMI) shielding of two dimensional (2D) MXene and graphene aerogel composites. *Nanomaterials.* 2020;10(4):702.
230. Alhabeab M, Maleski K, Anasori B, et al. Guidelines for synthesis and processing of two-dimensional titanium carbide ( $\text{Ti}_3\text{C}_2\text{T}_x$  MXene). *Chem Mater.* 2017;29(18):7633-7644.
231. Ghidui M, Lukatskaya MR, Zhao M-Q, Gogotsi Y, Barsoum MW. Conductive two-dimensional titanium carbide 'clay' with high volumetric capacitance. *Nature.* 2014;516(7529):78-81.
232. Lee Y, Kim SJ, Kim YJ, et al. Oxidation-resistant titanium carbide MXene films. *J Mater Chem A.* 2020;8(2):573-581.
233. Iqbal A, Hong J, Ko TY, Koo CM. Improving oxidation stability of 2D MXenes: synthesis, storage media, and conditions. *Nano Converg.* 2021;8(1):1-22.
234. Xu X, Chen Y, He P, et al. Wearable  $\text{CNT}/\text{Ti}_3\text{C}_2\text{T}_x$  MXene/PDMS composite strain sensor with enhanced stability for real-time human healthcare monitoring. *Nano Res.* 2021;14(8):2875-2883.
235. Li X, He L, Li Y, et al. Healable, degradable, and conductive MXene nanocomposite hydrogel for multifunctional epidermal sensors. *ACS Nano.* 2021;15(4):7765-7773.

## AUTHOR BIOGRAPHIES



**Abbas Ahmed** is a PhD student under the guidance of Prof. Luyi Sun in Polymer Program at the Institute of Materials Science, University of Connecticut, USA. He received his Bachelor's degree in Textile Engineering from the University of Dhaka, Bangladesh, in 2018. His primary research focuses on nanostructured and bioinspired material devised flexible nanoelectronics and soft-robotics for smart-textiles, healthcare, and energy-related applications.



**Samrat Mukhopadhyay** is an Associate Professor at the Department of Textile and Fiber Engineering, Indian Institute of Technology (IIT), Delhi. He received his BSc (Tech) from the University of Kolkata, and subsequently did his Masters and PhD from IIT Delhi, India. He was with the Fibrous Materials Research Group at the University of Minho, Portugal as a Post-Doctoral Scientist before joining the Department. He has been working with synthetic and natural fibers, composite materials, sustainable approaches in textiles and in the revival of traditional textiles.



**Luyi Sun** received his BS from South China University of Technology in 1998 and PhD from the University of Alabama (advisor: Prof. Joseph Thrasher) in 2004. After his postdoctoral training at Texas A&M University (supervisors: Profs. Hung-Jue Sue and Abraham Clearfield), he worked at TOTAL Petrochemicals USA, Inc. from 2006 to 2009. He was an Assistant Professor at Texas State University from 2009 to 2013. Dr. Sun joined the University of Connecticut as an Associate Professor in 2013 and was promoted to Professor in 2018. His research focuses on the design and synthesis of nanostructured materials for various applications.

**How to cite this article:** Ahmed A, Sharma S, Adak B, et al. Two-dimensional MXenes: New frontier of wearable and flexible electronics. *InfoMat.* 2022;4(4):e12295. doi:10.1002/inf2.12295